Superconductivity in Layered BiS_2-Based Compounds

D. Yazici[a,b], I. Jeon[b,c], B. D. White[a,b], M. B. Maple[a,b,c,*]

[a] *Department of Physics, University of California, San Diego, La Jolla, California 92093, USA*
[b] *Center for Advanced Nanoscience, University of California, San Diego, La Jolla, California 92093, USA*
[c] *Materials Science and Engineering Program, University of California, San Diego, La Jolla, California 92093, USA*

Abstract

A novel family of superconductors based on BiS_2-based superconducting layers were discovered in 2012. In short order, other BiS_2-based superconductors with the same or related crystal structures were discovered with superconducting critical temperatures T_c of up to 10 K. Many experimental and theoretical studies have been carried out with the goal of establishing the basic properties of these new materials and understanding the underlying mechanism for superconductivity. In this selective review of the literature, we distill the central discoveries from this extensive body of work, and discuss the results from different types of experiments on these materials within the context of theoretical concepts and models.

Keywords: BiS_2-based compounds, Superconductivity
PACS: 74.25.F-, 74.62.Dh, 74.62.Fj, 74.62.-c

1. Introduction

The 2012 discovery [1] of superconductivity with transition temperature T_c = 8.6 K in $Bi_4O_4S_3$ captured the attention of physicists and chemists worldwide. This compound has a layered crystal structure composed of superconducting BiS_2 layers and spacer layers of $Bi_4O_4(SO_4)_{1-x}$, where x indicates the defects of SO_4 ions at the interlayer sites. The crystal structure is shown in Fig. 1(a). The layered crystal structure is analogous to those of high-temperature (high-T_c) cuprate and Fe-based superconductors in which T_c can be tuned by varying the blocking layers [2, 3, 4, 5]. By modifying the blocking layer in $Bi_4O_4S_3$, superconductivity was discovered in the BiS_2-based compound $LaO_{0.5}F_{0.5}BiS_2$ [6]. The two distinct crystal structures among this class of materials are compared in Fig. 1. The basal plane of the $Bi_4O_4(SO_4)_{1-x}$ and $LnOBiS_2$ (Ln = lanthanide) compounds at room temperature is displayed in Fig. 2. Both structures are composed of an alternate stacking of the two BiS_2 double layers and the blocking layer. Electron carriers, which are essential for the emergence of superconductivity in the BiS_2-based superconductors, can be generated by modifying the structure and the chemical composition at the blocking layers. In the $LnOBiS_2$ compounds, electron carriers can be generated by a partial substitution of O^{2-} by F^- [1, 7, 8], which is an electron-doping strategy that is commonly used in the Fe-pnictides [9, 4, 5]. These findings motivated the scientific community to try other ways of altering the blocking layers and, shortly after the discovery of superconductivity in $LaO_{0.5}F_{0.5}BiS_2$, it was found that replacing nonmagnetic La with magnetic rare-earth elements (Ce, Pr, Nd, Yb) substantially increased T_c [10, 8] to its current record of 5.4 K for this crystal structure [8]. It has also been found that superconductivity in the $LaOBiS_2$ system can be induced by increasing the charge-carrier density (electron doping) through substitution of tetravalent elements, i.e., Ti, Zr, Hf, and Th, for trivalent La [11]. By electron doping, the parent phases of $LaOBiS_2$ and $ThOBiS_2$, considered to be bad metals, become superconducting with T_c up to 2.85 K. On the other hand, hole doping by substitution of divalent Sr for trivalent La did not induce superconductivity in those materials [11]. Recently, superconductors with $BiSe_2$ conduction layers were discovered. It has been reported that $LaO_{0.5}F_{0.5}BiSe_2$, with a crystal structure similar to $LaOBiS_2$ exhibits superconductivity below T_c = 2.6 K [12, 13, 14]. A selection of T_c values obtained at ambient pressure for the known BiS_2-based superconductors is listed in Table 1.

Applying external pressure reduces the T_c for $Bi_4O_4S_3$ [15, 16] while it increases the T_c for $LnO_{1-x}F_xBiS_2$ (Ln = La, Ce, Pr, Nd) [15, 17, 18, 19]. This is another similarity to the Fe-based superconductors; T_c is sensitive to applied pressure [4, 9, 5]. A comparison between the crystal and electronic structures of the BiS_2- and Fe-based superconductors reveals many broad similarities. Theoretical considerations of the density of states, band structure, and Fermi surface nesting, studied by means of first principles calculations, indicated that the insulating $LaOBiS_2$ parent phase (band gap of 0.15 eV) transforms into a metallic state after chemical substitution with fluorine [20, 21, 22]. At the optimal concentration (x = 0.5), four bands originating from Bi p_x and p_y orbitals cross the Fermi level. The surface nesting of $LaO_{1-x}F_xBiS_2$ was found to be weaker than that of the iron-pnictide compound LaOFeAs [23].

The details concerning superconductivity in the BiS_2-based compounds are still under debate; some studies have even reported evidence indicating that superconductivity in $Bi_4O_4S_3$ is not a bulk phenomenon and might be associated with impurity

*Corresponding author
Email address: mbmaple@physics.ucsd.edu (M. B. Maple)

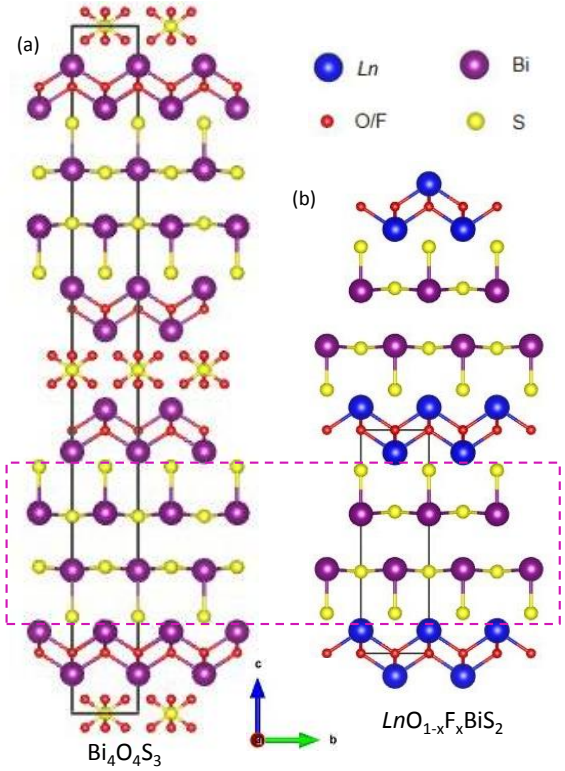

Figure 1: (Color online) Comparison of the crystal structures of (a) $Bi_4O_4S_3$ and (b) $LaO_{1-x}F_xBiS_2$. A box with dashed boundaries indicates the superconducting BiS_2 layers, which are common to both crystal structures.

phases instead [24, 25]. On the other hand, recent studies on single crystals of $LnO_{1-x}F_xBiS_2$ (Ln = La, Ce, Nd), grown by a flux method [26, 27, 28, 14], clearly confirm the bulk nature of superconductivity in these BiS_2-based layered materials.

About 83 experimental papers and 20 theoretical papers concerning BiS_2-based superconductivity have been published in peer-reviewed journals and/or posted on the arXiv [29] to date. Much of this research is driven by the following questions: What physical parameters determine T_c? Is new physics involved in the physical properties? What is the upper limit of T_c for this class of materials? Where should we look next to find new superconductors with high T_c values? Is the pairing mechanism similar to that in unconventional superconductors (i.e., Fe-based superconductors, cuprates, etc.) or is pairing more likely to be phonon mediated? Herein, we provide a selective review of the large and growing body of literature concerning BiS_2-based superconductors and related materials. In particular, we review the experimental results reported in the literature and discuss the relationships of the properties with one another and to T_c, making occasional reference to theoretical concepts and models. Although the superconducting properties are discussed, we emphasize the normal-state properties; in particular, special attention is given to the electronic and magnetic properties as determined from various studies, because of their potential connection to the pairing mechanism for superconductivity in these materials.

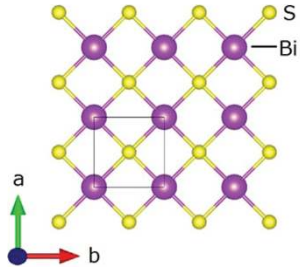

Figure 2: (Color online) Projection of a Bi-S layer onto the *ab*-plane. The structure of the Bi-S layer is identical for all superconducting BiS_2-based compounds.

Table 1: Superconducting transition temperatures T_c for all known BiS_2-based and related superconducting compounds. The T_c values were defined from the onset in electrical resistivity measurements.

Compound	T_c (K)	Ref.
$Bi_4O_4S_3$	4.4	[1, 30, 15, 31, 32, 33, 34, 35]
$LaO_{0.5}F_{0.5}BiS_2$	2.8	[6, 36, 8, 37, 15, 38, 39, 40, 41, 42]
$CeO_{0.5}F_{0.5}BiS_2$	3.0	[8, 43, 44, 27, 45]
$PrO_{0.5}F_{0.5}BiS_2$	3.5	[8, 46, 27, 47]
$NdO_{0.5}F_{0.5}BiS_2$	4.0	[10, 8, 26, 48, 49, 27, 22]
$YbO_{0.5}F_{0.5}BiS_2$	5.4	[8]
$La_{1-x}Ti_xOBiS_2$	2.4	[11]
$La_{1-x}Zr_xOBiS_2$	1.7	[11]
$La_{1-x}Hf_xOBiS_2$	2.4	[11]
$La_{1-x}Th_xOBiS_2$	2.0	[11]
$Sr_{1-x}La_xFBiS_2$	3.5	[50, 51]
$LaO_{0.5}F_{0.5}BiSe_2$	3.6	[12, 28, 14, 13]
$EuBiS_2F$	0.3	[52]

2. Structural properties

The reported x-ray diffraction pattern of $Bi_4O_4S_3$ includes peaks associated with Bi metal, Bi_2S_3, and a third phase with crystal structure characterized by a body-centered tetragonal unit cell characterized by either $I4/mmm$ or $I\bar{4}2m$ space groups. These space groups are not distinguishable in the x-ray diffraction pattern; however, because of the higher-symmetry, $I4/mmm$ with unit cell parameters of a = 3.9592(1) and c = 41.241(1) Å has been selected as the crystal structure of $Bi_4O_4S_3$ [1]. As shown in Fig. 1(a), the layered crystal structure is composed of Bi_2S_4 layers, Bi_2O_2 layers, and SO_4 units. The fluorite-type Bi_2O_2 layer is a common component in $I4/mmm$ or $P4/nmm$ tetragonal layered structures. The rocksalt-type Bi_2S_4 layer structure has been found only in $LnOBiS_2$ (Ln = Ce, Gd, and Dy) with the $P4/nmm$ space group [1]. Figure 2 depicts a projection of the Bi_2S_4 layer along the c axis. The Bi and S atoms form square lattices. The fact that superconductivity occurs within the square-lattice sheets resembles the CuO_2 and FeAs layers of high-T_c cuprates and Fe-pnictides/chalcogenides, respectively [2, 3, 53, 4, 9, 5, 54]. The elemental composition of this crystal structure can be described as $Bi_4O_4(SO_4)_{1-x}Bi_2S_4$, where x indicates the occupancy of the SO_4 unit site. When SO_4 sites are fully occu-

pied, the atomic composition should be $Bi_4O_4(SO_4)Bi_2S_4$, also denoted as $Bi_6O_8S_5$, with unit cell parameters a = 3.965(5) and c = 41.234(0) Å [55], which is an insulator according to band structure calculations [1, 21]. Superconductivity in $Bi_4O_4S_3$ is induced by electron doping into the BiS_2 layers via the introduction of vacancies into the SO_4 sites. There is a discrepancy of less than 5% and 7% in the lattice parameter values for a and c, respectively, among the various reports for $Bi_4O_4S_3$ [1, 33, 55, 24]. On the other hand, a slight distortion from the ideal square lattice of Bi-S atoms (see Fig. 2) has been reported for $Bi_4O_4S_3$ [55], which might suggest that the larger bending of the Bi-S-Bi bond is responsible for superconductivity. A similar distortion of the Bi-S layers in $LaO_{1-x}F_xBiS_2$, $CeO_{1-x}F_xBiS_2$, and $PrO_{0.5}F_{0.5}BiS_2$ has also been observed [36, 37, 56, 46]; the distortion of the Bi-S layers could be attributed to a fully occupied Bi s-orbital. Chemical substitution of F for O is considered to induce charge carriers into the Bi-S layer, and this is believed to induce superconductivity in the mixed-anion layered compounds $LnO_{1-x}F_xBiS_2$ (Ln = La, Ce, Pr, Nd, Yb) [6, 36, 8, 37, 15, 38, 39, 40, 41, 42]. The effect of F substitution on the lattice parameters and T_c has been reported for $LaO_{1-x}F_xBiS_2$ [36]. The experimental lattice parameters, determined from single-crystal and polycrystalline samples, are similar to those predicted by computational results up to $x \sim 0.5$. However, with increasing F concentration, the predicted lattice parameters show significant differences from the experimental values. Only the lattice parameter c of the polycrystalline sample prepared using high-pressure (HP) annealing follows the computed trend [57]. The crystal structures of $LaO_{1-x}F_xBiS_2$ for $x \sim 0.23$ (not superconducting) and 0.46 (superconducting) were determined by single-crystal x-ray diffraction analysis. Slightly corrugated and nearly flat Bi-S planes were found in $LaO_{1-x}F_xBiS_2$ at $x \sim 0.23$ and 0.46, respectively [57]. The increase in the F concentration changes the distortion of the Bi-S plane, and an almost flat Bi-S plane is observed at superconducting concentration $x \sim 0.46$. Since the in-plane distances are comparable for $x \sim 0.23$ and ~ 0.46, a nearly flat Bi-S plane should enhance hybridization of the Bi $6p_x/6p_y$ and S $3p_x/3p_y$ orbitals; therefore, F substitution not only increases the carrier concentration, it also changes the distortion of the Bi-S plane.

3. Band structure calculations

Several theoretical works addressing the band structure have been reported, especially for $LaO_{0.5}F_{0.5}BiS_2$ [6, 58, 59, 40, 20, 60, 61, 41, 62, 63, 64, 65, 66, 67]. The calculated band structures and electronic density of states (DOS) for $LaO_{1-x}F_xBiS_2$ with x = 0, 0.5, and 1 are shown in Fig. 3 [40]. The contribution of various orbitals to the band structure are characterized by different colors: blue (Bi-p), red (S1-p), and green (O-p and S2-p). For $LaOBiS_2$ (see Fig. 3(a)), the Fermi level is located at the upper edge of the valence bands with an energy gap of ~0.8 eV, indicating an insulating behavior. The valance bands spread from around −6 to 0 eV and consist of p-electron states from the O and S atoms. While the La-d and La-f electron states lie far above the Fermi level near 4 eV, Bi-p and S1-p states

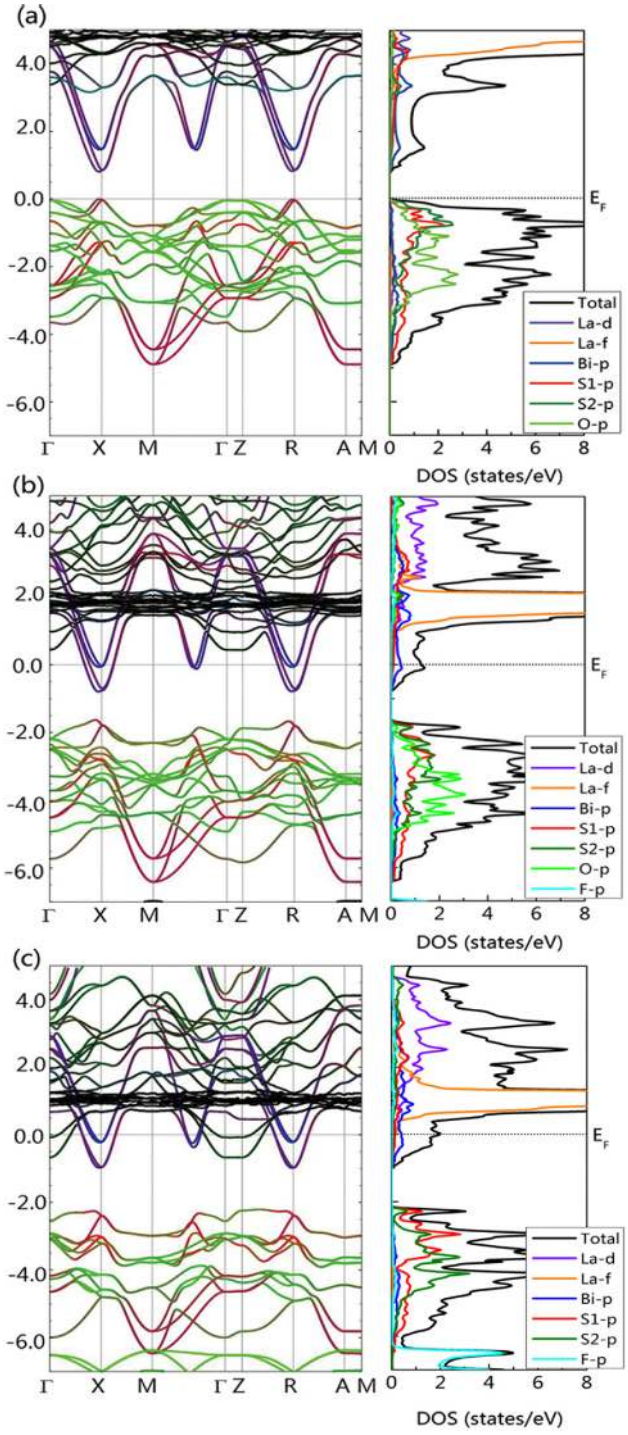

Figure 3: (Color online) Calculated band structure and density of states for $LaO_{1-x}F_xBiS_2$ with x = 0 (a), 0.5 (b), and 1 (c), with the orbital character indicated by different colors: Bi-p (blue), S1-p (red), O-p (light green), and S2-p (green) (after Li *et al.* [40]).

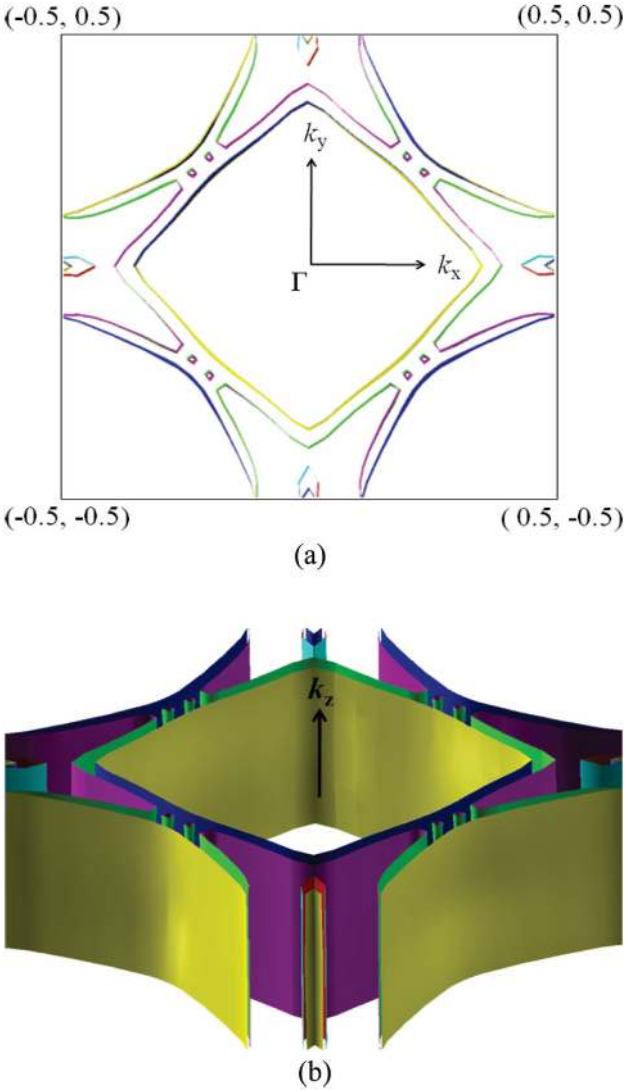

Figure 4: (Color online) The calculated Fermi surface of $LaO_{0.5}F_{0.5}BiS_2$: (a) cross section of Fermi surface for $k_z = 0$ and (b) a 3D perspective (after Wan *et al.* [58]).

dominate the conduction bands [40]. For $LaO_{0.5}F_{0.5}BiS_2$, the Fermi level crosses the conduction bands coming from the Bi-p and S1-p electron states, so that the Bi-S1 layers contribute strongly to electronic conduction. As shown in Fig. 3(b), the Fermi level crosses four bands creating electron pockets, and thus the charge carriers in $LaO_{0.5}F_{0.5}BiS_2$ are electrons [42]. The DOS at the Fermi level is equal to $N(E_F) = 1.22$ eV^{-1} per formula unit, and the corresponding bare susceptibility and specific heat coefficient are estimated $\chi_0 = 4.0 \times 10^{-5}$ emu/mol and $\gamma_0 = 3.0$ mJ/mol K^2, respectively. For $LaFBiS_2$ (see Fig. 3(c)), the Fermi level crosses the conduction bands and the energy gap between the conduction and valence bands increases to ~1.1 eV. Meanwhile, the DOS at the Fermi level increases to $N(E_F) = 1.84$ eV^{-1} per formula unit, yielding $\chi_0 = 6.0 \times 10^{-5}$ emu/mol and $\gamma_0 = 4.5$ mJ/mol K^2.

The calculated Fermi surface of $LaO_{0.5}F_{0.5}BiS_2$ is displayed in Fig. 4. It has been found that the bands crossing the Fermi level are from Bi-6p electron states and a two-band electronic model has been proposed based on the band-structure calculation [21]. Due to the quasi-one-dimensional nature of the conduction bands, Fermi surface nesting with wave vector $\mathbf{k} = (\pi, \pi, 0)$ has been observed [21]. The lattice dynamics and the electron-phonon interactions in $LaO_{0.5}F_{0.5}BiS_2$ have also been studied using density functional theory calculations [20, 58, 40]. It has been suggested that a charge-density-wave (CDW) instability around the M point is a possible consequence of the Fermi surface nesting [58]. However, no signatures for CDW instabilities have been observed in physical properties measurements, except for an inflection point in the electrical resistivity for $La_{0.9}M_{0.1}OBiS_2$ (M = Th, Ti, Zr, Hf); it was speculated that these features were associated with a CDW instability in these compounds [11]. Recently, it was reported by Zhai *et al.* that a CDW-like transition occurs in $EuBiS_2F$ at $T_{CDW} \sim 280$ K and superconductivity emerges at 0.3 K. It has been proposed that the mixed valence of Eu, in which a considerable amount of electrons are transferred into the conduction band, induces superconductivity and the CDW instability in $EuBiS_2F$ [52]. It has been suggested that BiS_2-based compounds are strong electron-phonon coupled superconductors in the vicinity of competing ferroelectric and CDW phases [20]. Density-functional linear response calculations give a large electron-phonon coupling constant ($\lambda \sim 0.8$), suggesting and that $LaO_{1-x}F_xBiS_2$ as a strong electron-phonon coupled conventional superconductor.

Despite the results from band-structure calculations, some studies have emphasized the importance of electron-electron interactions and the possibility of unconventional superconductivity in BiS_2-based compounds [59, 63, 41, 65, 68]. Starting from a two-orbital model, spin/charge-fluctuation-mediated pairing interactions have been studied by using the random phase approximation [59, 63], and an extend s- or d-wave pairing has been proposed [63]. With the assumption that the pairing is a relatively short-range interaction, Liang *et al.* find that the extended s-wave pairing symmetry is very robust [41]. The possibility of triplet pairing and weak topological superconductivity has also been suggested based on renormalization-group numerical calculations [65]. It has also been proposed that BiS_2-based superconductors possess type-II two-dimensional Van Hove singularities, and the logarithmically-divergent DOS may induce unconventional superconductivity [68, 69].

To summarize, first-principles calculations indicate that $LaO_{1-x}F_xBiS_2$ changes from a band insulator at $x = 0$ to a band metal via chemical substitution (electron doping). Similar to the compound $LaFeAsO_{1-x}F_x$, electrons in $LaO_{1-x}F_xBiS_2$ are transferred from the LaO(F) blocking layer into the superconducting BiS_2 layers. The p-orbital states of Bi-S1 layers play an important role since they are the dominant contribution to the DOS at the Fermi level. From the phonon calculations for $LaO_{0.5}F_{0.5}BiS_2$, a strong electron-phonon coupling of $\lambda = 0.8$ has been obtained. A T_c of 9.1 K has been predicted using this value of λ, which is very close to the experimental value. This result is compelling evidence that $LaO_{0.5}F_{0.5}BiS_2$ is a conventional electron-phonon superconductor with phonon-mediated pairing. For $LaO_{1-x}F_xBiS_2$ [9, 5, 54], the electronic states

near the Fermi level are primarily from the hybridized p orbital states of the Bi and S1 atoms, and the electron-phonon coupling comes mainly from the contribution of optical phonon modes around the M and A points at the low-frequency branches. These results indicate that the BiS_2 layers play an important role in the transport and superconducting properties, similar to the CuO_2 layers of the cuprates or Fe-As layers of the Fe-based superconductors.

4. Neutron scattering

Neutron diffraction measurements have been performed on polycrystalline samples of the superconducting $LaO_{0.5}F_{0.5}BiS_2$ and its non-superconducting parent compound $LaOBiS_2$. Figure 5(a) shows neutron diffraction data and Rietveld refinements obtained from a powdered sample of $LaOBiS_2$. The nuclear Bragg peaks are within instrumental-resolution limits, indicating good crystallinity. On the other hand, Bragg peaks from the superconducting $LaO_{0.5}F_{0.5}BiS_2$ sample, which are displayed in Fig. 5(b), exhibit pronounced broadening compared to those from the non-superconducting $LaOBiS_2$ sample; this indicates imperfect crystallinity. In both compounds, discrepancies between experimental and calculated structural parameters have been observed, which suggest inherent structural instabilities in these systems [20, 39].

It was theoretically predicted that, in the superconducting phase, a significant change in the phonon DOS at low energies would occur due to a potentially large electron-phonon coupling [20, 58, 40]. However, inelastic neutron scattering data yield no considerable changes in the low-energy phonon modes as the system becomes superconducting either by F substitution or by cooling through the superconducting transition [39].

5. Hall effect and magnetoresistance

It is well known that the normal-state properties, such as the Hall effect and magnetoresistance, are very important to understand the primary electron scattering contributions, which are often intimately related to the mechanism underlying superconductivity. For instance, the linear temperature dependence of the electrical resistivity and the fact that the Hall coefficient has a temperature dependence suggest an unconventional metallic state in cuprate superconductors that cannot be described as a Fermi liquid [2, 3, 53].

In order to elucidate the normal-state transport properties, Hall effect measurements were performed on $Bi_4O_4S_3$ by several groups [40, 34, 33]. A weak insulating behavior is induced in the normal state in a magnetic field. This can be induced either by an adjacent competing order, or the very shallow p_x and p_y bands and a small Fermi energy. The transverse electrical resistivity ρ_{xy} remains negative at all temperatures, indicating the electron-like charge carriers are dominant. The Hall coefficient R_H was determined using the formula $R_H = \rho_{xy}/H$, which is field-dependent, and the carrier concentration at low magnetic field was estimated to be $n \sim 1.53 \times 10^{19}$ cm^{-3} at 10 K, which increases to $\sim 2.4 \times 10^{19}$ cm^{-3} at 300 K [31, 33].

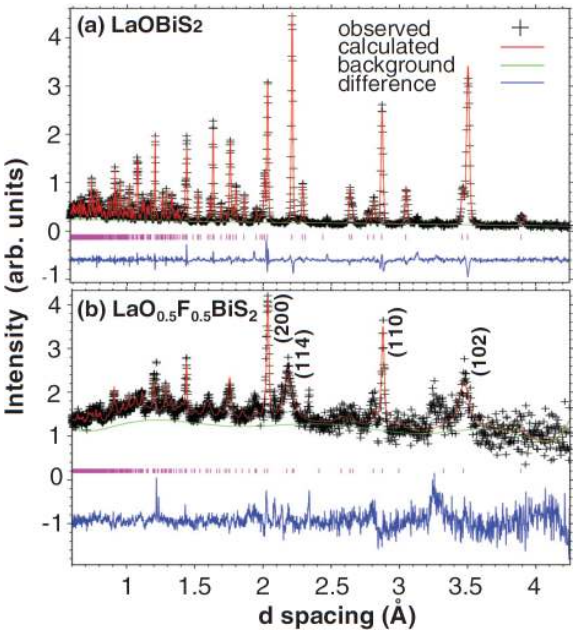

Figure 5: (Color online) Powder neutron diffraction data for (a) $LaOBiS_2$ and (b) $LaO_{0.5}F_{0.5}BiS_2$ at 15 K. Black crosses represent observed data. Red, green, and blue solid lines are the calculated intensity, estimated background, and difference between the observed and calculated intensities obtained by GSAS [70], respectively (after Lee *et al*. [39]).

The magnetic field dependence of ρ_{xy} exhibits non-linear behavior at all temperatures, prohibiting any single-band description within the context of Fermi liquid theory. Both the strong non-linear Hall effect and the magnetoresistance are consistent with a multiband character as expected from the theoretical calculations [40, 21]. Unlike $Bi_4O_4S_3$, the magnetic field dependence of ρ_{xy} for $LaO_{0.5}F_{0.5}BiS_2$ exhibits a linear response at low magnetic fields [42]. The charge carriers are primarily electrons and the calculated Hall coefficient and carrier concentration at $T = 10$ K are $n = 1.24 \times 10^{20}$ cm^{-3} and $R_H = 5.04036 \times 10^8$ m^3/C, respectively. The carrier concentration is about one order of magnitude higher than in $Bi_4O_4S_3$ [42]. However, to unravel the different scattering rates from the distinct bands in a multiband system, a high magnetic field is required; without a large magnetic field, only the scattering from partial bands is detected. Hall effect and magnetoresistance measurements for $CeO_{1-x}F_xBiS_2$ (x = 0, 0.25, and 0.5) suggested that the parent phase is a bad metal instead of a band insulator, which is also suggested by the LDA calculation [10]. By substituting F with O, superconductivity gradually emerges along with a semiconducting-like normal state. The magnetic field dependence of ρ_{xy} exhibits more curvature at low doping levels. This illustrates that there may be a very strong multiband or a shallow band-edge effect at these concentrations. With further doping, the nonlinear curvature seems to weaken slightly. The multiband effects, determined from the non-linear magnetic field dependence of ρ_{xy} for BiS_2-based compounds [31, 33, 71, 72], might also be related with spin density wave (SDW) or CDW formation [73], which is also suggested by first-principles calculations [20]; there is either a CDW insta-

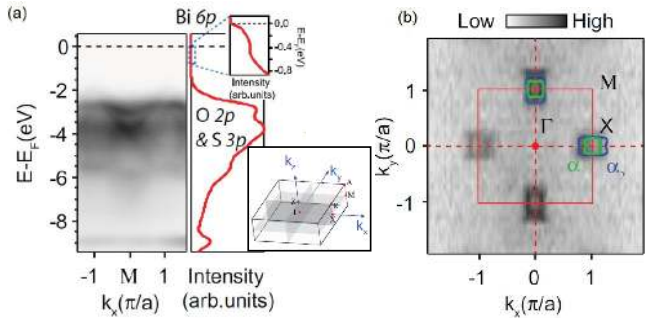

Figure 6: (Color online) (a) The valence band structure around the M point along the $M - X$ direction and corresponding angle-integrated energy distribution curves (EDCs). The inset is an enlarged view of the features near E_F. The three-dimensional Brillouin zone of $NdO_{0.5}F_{0.5}BiS_2$ is displayed in the right corner of the figure. (b) The photoemission intensity map of $NdO_{0.5}F_{0.5}BiS_2$ at E_F over the projected two-dimensional Brillouin zone, which was obtained through mirroring the data with respect to the k_x and k_y axes. The intensity was integrated over an energy window of (E_F - 15 meV, E_F + 15 meV). The Fermi surface sheets for the α_1 (along the $\Gamma - X$ direction) and α_2 bands are shown by the rectangles with different colors. The data were measured using 100 eV photons (after Ye *et al*. [74]).

bility or an enhanced correlation effect in this system.

6. ARPES measurements

Angle-resolved photoemission spectroscopy (ARPES) is a powerful experimental probe, with its unique capability to directly image electronic structures of materials in energy-momentum space. Figure 6 shows the results from ARPES studies on a single crystal of $NdO_{0.5}F_{0.5}BiS_2$ with T_c of 4.87 K by Ye *et al*. [74]. Figure 6(a) shows the valence band structure around the X point along the M - X high symmetry direction at 15 K. The features between -5 to -1 eV are mainly from O $2p$ and S $3p$ electron state contributions [58], while the small spectral weight near E_F can be assigned to the Bi $6p$ state. Figure 6(b) displays the photoemission intensity map of $NdO_{0.5}F_{0.5}BiS_2$, which is overlaid on the two-dimensional Brillouin zone. Here, the unit of k_x and k_y is π/a, where a is the neighboring Bi-Bi distance in the Bi-S plane. Two rectangular Fermi pockets were observed around X with little k_z dependence in the Brillouin zone, which is direct evidence for a multiband character in this compound. This is consistent with the previous Hall effect measurements and theoretical studies as well [71, 21, 33, 40].

Based on the Luttinger theorem [75, 76], the number of charge carriers in this system is estimated to be consistent with a fluorine concentration $x = 0.16 \pm 0.02$, which deviates significantly from the nominal composition of $x = 0.5$. However, band-theory calculations also show that the calculated Fermi surface for $x = 0.16$ agrees with the experimentally-determined Fermi surface as displayed in Fig. 7, which is likely due to a bismuth deficiency. This gives much smaller Fermi pockets than those predicted by theoretical calculations for the nominal composition. The small Fermi pocket size and the weak electron correlations obtained in these experiments suggest that

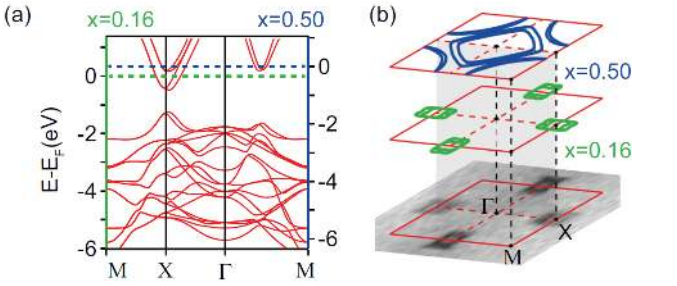

Figure 7: (Color online) (a) The calculated band structures without spin-orbit coupling for $NdO_{0.84}F_{0.16}BiS_2$ (the left vertical axis) and $NdO_{0.5}F_{0.5}BiS_2$ (the right vetical axis). (b) A comparison of the Fermi surface between the photoemission intensity map and density-functional theory calculations for $x = 0.5$ and $x = 0.16$ (after Ye *et al*. [74]).

the BiS_2-based compounds could be conventional BCS superconductors, mediated by the electron-phonon coupling.

7. Soft x-ray photoemission spectroscopy

Soft x-ray photoemission spectroscopy (SXPES) measurements yield a spectrum that reflects the bulk valence band DOS and core levels, and are therefore a suitable probe of the electronic structure and the chemical state of solids. The electronic structure of $LaO_{1-x}F_xBiS_2$ (x = 0, 0.3, 0.5) is investigated via core-level and valence-band SXPES measurements [77]. The core-level spectra of doped samples shows a new spectral feature at the lower binding energy side of the Bi $4f$ main peak as presented in Fig. 8. This feature may be explained by core-hole screening with metallic states near the Fermi level (E_F). The experimental electronic structure and its x dependence (shift of the valence band to higher binding energy as well as the appearance of new states near E_F having dominant Bi $6p$ character) were found to be consistent with the predictions from band structure calculations. On the other hand, an obvious deviation of the intensity and spectral shape of the states near E_F from those of calculations was observed. Figure 9 shows the valence band SXPES spectra for $LaO_{1-x}F_xBiS_2$ (x = 0, 0.3, 0.5), obtained using 500 eV photons (open circles connected with lines), together with that of $LaO_{0.5}F_{0.5}BiS_2$ with 1100 eV photons (broken line). The valence band spectrum of $LaOBiS_2$ (x = 0) has a peak around 2.5 eV with structure near 5 eV. The spectrum shows a negligible intensity region from E_F to a 1 eV binding energy, which indicates an experimental band gap of 1 eV below E_F. As x increases, the whole valence band shifts to higher binding energy by ~0.3 eV, as seen in the shift of the spectral edge of the valence band around 2 eV. The x-dependent shift to higher binding energy is consistent with electron doping by substitution of F with O. Regarding the spectral shape, the structure around 5 eV gets broader and a new peak evolves around 8.5 eV; the latter peak also shifts to higher binding energy. Absence of the peak around 8.5 eV in the $x = 0$ sample and its systematic evolution indicate that the structure is driven by chemical substitution. Importantly, it is observed that the intensity near E_F increases with x. According to band-structure calculations [58, 20, 40], $LaOBiS_2$ has a valence band derived

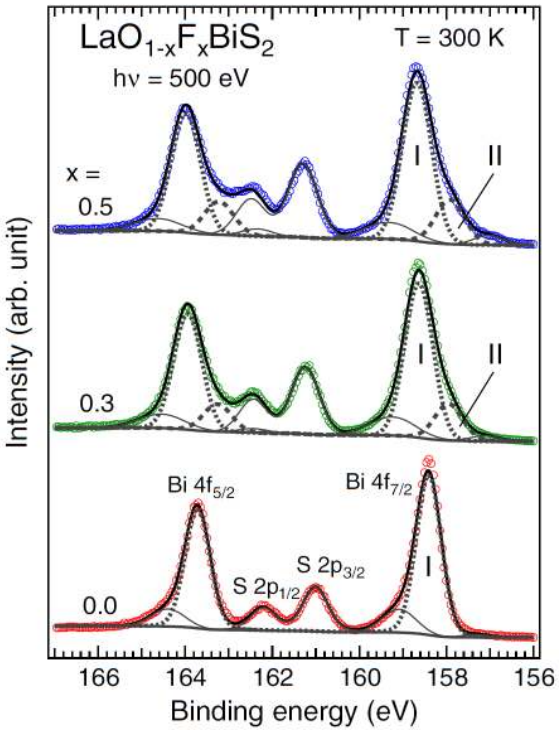

Figure 8: (Color online) Bi 4f and S 2p core level soft x-ray photoemission spectroscopy data for $LaO_{1-x}F_xBiS_2$ (x = 0, 0.3, 0.5) (open circles) and the results of fitting (curves). The spectra were normalized to the intensity of the Bi $4f_{7/2}$ feature (after Nagira *et al.* [77]).

from S (S1 and S2), 3p, and O 2p orbitals with a ~4 eV band width, which is separated by a band gap of ~0.8 eV from the bottom of the highly-dispersive conduction band of dominant Bi $6p_{x,y}$ character that is hybridized with S1 3p electron states. Electrons introduced by substitution of F for O fill the conduction band and, for x = 0.5, E_F is expected to be located at ~0.8 eV above the bottom of the conduction band. For x = 0, the fact that the experimental band gap of 1 eV below E_F is comparable to that of the calculated band gap suggests that E_F may be located near the bottom of the conduction band, possibly due to impurity and/or self doping [71]. Assuming that E_F for x = 0 is located at the bottom of the conduction band, a chemical potential shift of ~0.3 eV between x = 0 and 0.5 can be inferred. This value is a factor of 2 smaller than that expected from band-structure calculations (0.8 eV). Comparing this observation with band-structure calculations, it is likely that the valence band is dominated by S 3p and O 2p electron states. The bottom of the conduction band is mainly derived from Bi $6p_{x,y}$ and S1 3p electron states. The peak around 8.5 eV is ascribed to F 2p electron states.

8. Specific heat

Plots of specific heat divided by temperature C/T vs. T for $LnO_{0.5}F_{0.5}BiS_2$ (Ln = La, Ce, Pr, Nd, Yb) are shown in Fig. 10(a). There is no clear jump at their respective T_c's as determined from $\rho(T)$ and magnetic susceptibility $\chi(T)$ measurements. Instead, a Schottky-like anomaly is observed below ~6

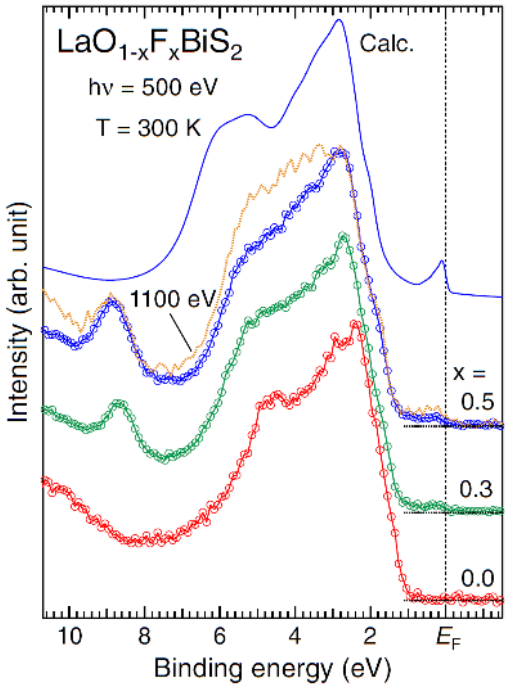

Figure 9: (Color online) Valence band soft x-ray photoemission spectroscopy data for $LaO_{1-x}F_xBiS_2$ (x = 0, 0.3, 0.5) obtained using 500 eV (open circles connected with lines) and 1100 eV (broken line) incident photon energies (only for $LaO_{0.5}F_{0.5}BiS_2$). All spectra measured with a 500 eV photon energy were normalized to the intensity of the peak around 2 - 3 eV binding energy. The 1100 eV spectrum was normalized to the 500 eV one for the x = 0.5 sample using the intensity of the peak around 3 eV. A spectrum for a 500 eV incident photon energy, based on calculated density of states for x = 0.5, is also shown, for which the energy resolution, lifetime broadening, and Fermi-Dirac distribution function at 300 K were taken into account (after Nagira *et al.* [77]).

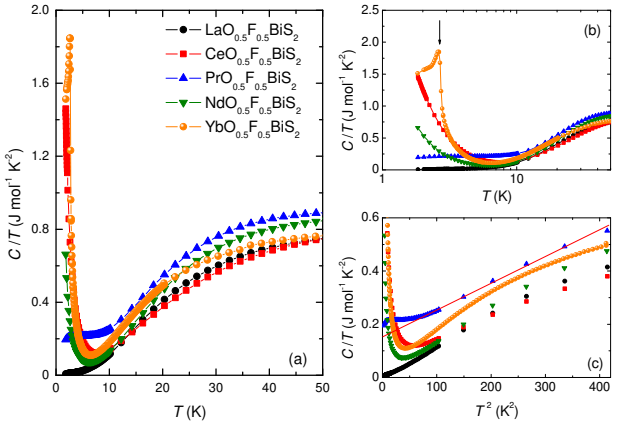

Figure 10: (Color online) (a) Specific heat divided by temperature C/T vs. T for $LnO_{0.5}F_{0.5}BiS_2$ (Ln = La, Ce, Pr, Nd, Yb). (b) Semi-log plot of $LnO_{0.5}F_{0.5}BiS_2$. The arrow indicates the magnetic ordering temperature for $YbO_{0.5}F_{0.5}BiS_2$. (c) C/T vs. T^2 for $LnO_{0.5}F_{0.5}BiS_2$. The red solid line represents a fit to the data for $PrO_{0.5}F_{0.5}BiS_2$ using the equation $C/T = \gamma + \beta T^2$.

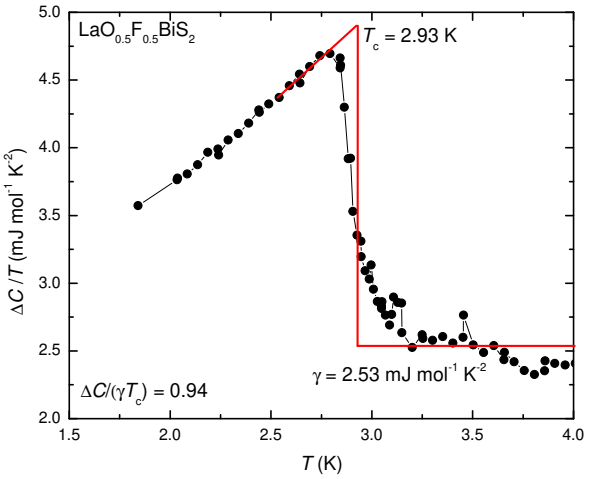

Figure 11: (Color online) A plot of $\Delta C/T$ where ΔC is the electronic contribution to the specific heat, in the vicinity of the superconducting transition. An idealized entropy conserving construction yields T_c = 2.93 K and $\Delta C/\gamma T_c$ = 0.94 (after Yazici *et al.* [8]).

K for $PrO_{0.5}F_{0.5}BiS_2$ and magnetic order (probably antiferromagnetic order) is observed at ~2.7 K (indicated by an arrow in Fig. 10(b)) that apparently coexists with superconductivity below 5.4 K for $YbO_{0.5}F_{0.5}BiS_2$ [8]. There is an upturn in C/T vs. T data at low temperature for $CeO_{0.5}F_{0.5}BiS_2$ that is consistent with the ferromagnetic ordering temperature T_C determined by Xing *et al.* [71]. The upturn in C/T vs. T data at low temperature for $NdO_{0.5}F_{0.5}BiS_2$ may also indicate the presence of incipient magnetic order. These results suggest that any anomaly around T_c may be overwhelmed by the large specific heat contributions associated with magnetic order for $CeO_{0.5}F_{0.5}BiS_2$, $NdO_{0.5}F_{0.5}BiS_2$, and $YbO_{0.5}F_{0.5}BiS_2$ and the Schottky-like feature for $PrO_{0.5}F_{0.5}BiS_2$.

The electronic and phonon contributions to specific heat, characterized by the Sommerfeld coefficient γ and coefficient β, respectively, were determined by performing linear fits to the data plotted as C/T vs. T^2 using the expression $C/T = \gamma + \beta T^2$. The fits were performed in the temperature range ~40-400 K^2 to avoid contributions from magnetic order or Schottky anomalies. The Debye temperature, Θ_D, was calculated using the relation $\beta = 12\pi^4 rR/(5\Theta_D^3)$ where $r = 5$ is the number of atoms per formula unit, and R is the universal gas constant. Values for γ are listed in Table 2. These values of γ are upper limits, and their precise values are subject to some uncertainty because of constraints imposed by the low-temperature upturns in the C/T vs. T for $CeO_{0.5}F_{0.5}BiS_2$ and $NdO_{0.5}F_{0.5}BiS_2$ and a Schottky-like anomaly for $PrO_{0.5}F_{0.5}BiS_2$.

An example of the linear fit of the C/T vs. T^2 data for $PrO_{0.5}F_{0.5}BiS_2$ is shown in Fig. 10(c) as a solid line. The value of γ for $LaO_{0.5}F_{0.5}BiS_2$ is consistent with the theoretically calculated $\gamma \sim 3.0$ mJ/mol K^2 [40]. On the other hand, one can see from the γ values listed in Table 2 that the electronic correlations are enhanced for the $4f$ rare-earth-based compounds relative to $LaO_{0.5}F_{0.5}BiS_2$, suggesting significant hybridization between Ln-$4f$ (Ln = Ce, Pr, Nd, Eu, Yb) and Bi-$6p$ electrons.

8.1. Specific Heat Jump at T_c

An important thermal property associated with bulk superconductivity in a material is the 'jump' ΔC in the electronic component of the specific heat at T_c. A nearly discontinuous increase in C at T_c only occurs if a sample has a single well-defined T_c that is not smeared out due to inhomogeneities, disorder, or other sample-quality issues. For BiS_2-based superconductors, it is uncommon to observe a clear jump in specific heat data at T_c. There is a tiny jump observed for a polycrystalline sample of $Bi_4O_4S_3$ which is consistent with its small electronic-specific-heat coefficient $\gamma \sim 2.8$ mJ/mol K^2. The specific-heat jump at T_c was determined to be $\Delta C/T_c = 4.0$ mJ/mol K^2 [35]. A clear jump has only been observed for a polycrystalline sample of $LaO_{0.5}F_{0.5}BiS_2$ [8]. The electronic contribution to the specific heat, $C_e(T) = C(T) - \beta T^3$, is shown in Fig. 11, which has been estimated by subtracting the lattice contribution βT^3 from $C(T)$. There is a clear jump at $T_c = 2.93$ K, determined from an idealized entropy conserving construction as shown in Fig. 11. This value of T_c is close to the temperature where the electrical resistivity of $LaO_{0.5}F_{0.5}BiS_2$ vanishes. The presence of the jump clearly indicates the bulk nature of superconductivity in this compound. The ratio of the jump to γ, $\Delta C/\gamma T_c = 0.94$, was calculated using a jump of $C_e/T = 2.37$ mJ/mol K^2 as seen in Fig. 11. This value for $\Delta C/\gamma T_c$ is less than the value of 1.43 predicted by the BCS theory, but is of the correct order of magnitude. The value of $\Delta C/\gamma T_c$ is evidently sensitive to the sample homogeneity and quality, which also determines the width of the transition. For this reason, the difficulty of preparing phase-pure specimens has made it challenging to unambiguously identify and study the intrinsic superconducting properties of BiS_2-based compounds via specific-heat measurements. Similar small values for $\Delta C/\gamma T_c$ have been observed in $Sr_{0.5}La_{0.5}FBiS_2$,

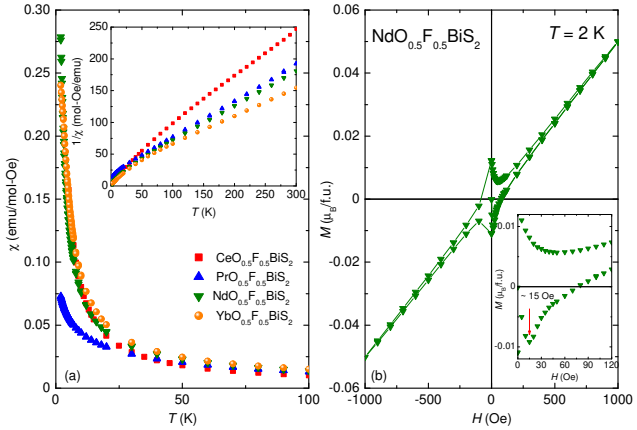

Figure 12: (Color online) (a) Magnetic susceptibility, $\chi = M/H$, as a function of temperature, T, measured in an applied magnetic field of $\mu_0 H = 0.1$ T for $Ln O_{0.5}F_{0.5}BiS_2$. Inset: Inverse magnetic susceptibility data, $\chi^{-1} = H/M$ vs. T, for $Ln O_{0.5}F_{0.5}BiS_2$. (b) M vs. H data at $T = 2$ K for $NdO_{0.5}F_{0.5}BiS_2$. Inset: Low-field M vs. H data at $T = 2$ K for $NdO_{0.5}F_{0.5}BiS_2$. An arrow indicates the critical magnetic field H_{c1} for $NdO_{0.5}F_{0.5}BiS_2$.

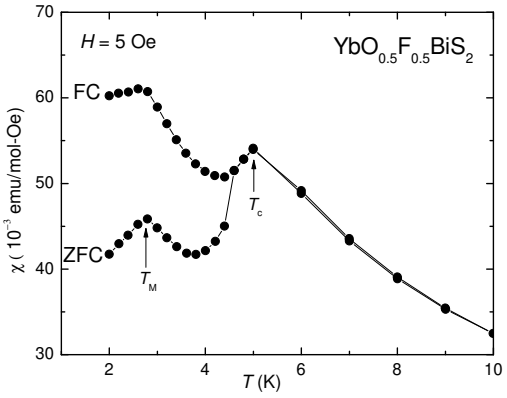

Figure 13: (Color online) Magnetic susceptibility, $\chi = M/H$, as a function of temperature, T, measured in an applied magnetic field of $H = 5$ Oe for $YbO_{0.5}F_{0.5}BiS_2$. Superconducting critical and magnetic ordering temperatures, T_c and T_M, respectively, are indicated by arrows for $YbO_{0.5}F_{0.5}BiS_2$ (after Yazici *et al.* [8]).

$LaO_{1-x}F_xBiS_2$, $La_{1-x}Y_xO_{0.5}F_{0.5}BiS_2$, $La_{1-x}Sm_xO_{0.5}F_{0.5}BiS_2$ and $La_{1-x}M_xOBiS_2$ systems [11, 50, 78, 79], and their values are listed in Table 2.

9. Susceptibility

Magnetic susceptibility $\chi = M/H$ data are displayed as a function of temperature in Fig. 12(a). Measurements were performed in applied magnetic field of $\mu_0 H = 0.1$ T for $Ln O_{0.5}F_{0.5}BiS_2$ (Ln = Ce, Pr, Nd, Yb) between 2 and 300 K. The $Ln O_{0.5}F_{0.5}BiS_2$ (Ln = Ce, Pr, Nd, Yb) compounds exhibit a Curie-Weiss-like $\chi(T)$ behavior with no noticeable anomalies indicative of any magnetic order down to 2 K. The χ^{-1} vs. T data, which are displayed in the inset of Fig. 12(a) for $Ln O_{0.5}F_{0.5}BiS_2$ (Ln = Ce, Pr, Nd, Yb), were fitted using a Curie-Weiss law,

$$\chi - \chi_0 = \frac{C_0}{(T - \Theta_{CW})}, \qquad (1)$$

in the temperature range ~20 - 300 K to determine the Curie-Weiss temperature Θ_{CW}. The effective magnetic moment μ_{eff} associated with the Ln ions was extracted from the Curie constant $C_0 = N_A \mu_{eff}^2 / 3k_B$, where N_A is Avogadro's number and k_B is Boltzmann's constant. The fits of Eq. (1) to the data were performed using a non-linear least squares regression. The resulting best-fit parameter values for μ_{eff} and Θ_{CW} are tabulated in Table 2, which are close to the theoretical Ln^{3+} free-ion values. This indicates that the $4f$ electrons are well localized in these compounds. However, the effective magnetic moment μ_{eff} for Eu in $EuBiS_2F$ was determined to be 7.2 μ_B /*f.u.*, which suggests a mixed valence for the Eu ion of about +2.2 [52].

The M vs. H data, measured at 2 K for $NdO_{0.5}F_{0.5}BiS_2$ and shown in Fig. 12(b), indicates that the superconductivity can be classified as type-II superconductivity with a mixed state. In the inset of Fig. 12(b), a critical magnetic field $H_{c1} = 15$ Oe is denoted by an arrow for $NdO_{0.5}F_{0.5}BiS_2$.

Zero-field cooled (ZFC) and field-cooled (FC) measurements of the magnetic susceptibility $\chi(T)$ were performed in a magnetic field of $H = 5$ Oe for the $Ln O_{0.5}F_{0.5}BiS_2$ (Ln = La, Ce, Pr, Nd, Yb) samples [8]. ZFC measurements yielded diamagnetic signals with T_c onset values that are consistent with the $\rho(T)$ data, while FC measurements reveal hardly any change in $\chi(T)$ in the superconducting state relative to the normal state, indicating strong vortex pinning. In contrast, both the ZFC and FC $\chi(T)$ data for $YbO_{0.5}F_{0.5}BiS_2$ reveal changes in behavior upon entering the superconducting state as well as hysteresis at T_c and peaks, indicated by an arrow in Fig. 13, near ~2.7 K that appear to be due to the magnetic order. This interpretation is further supported by a sharp feature in the specific heat data near ~2.7 K that is shown in Fig. 10(b). Magnetic ordering in $YbO_{0.5}F_{0.5}BiS_2$ is probably antiferromagnetic in nature, since superconductivity persists to temperatures below ~2.7 K and appears to coexist with the magnetic order. However, further study will be necessary to unambiguously characterize the order observed in $YbO_{0.5}F_{0.5}BiS_2$.

9.1. *Ferromagnetic order in $CeO_{1-x}F_xBiS_2$*

Even though experimental results [38, 80, 74] and theoretical models [41, 20] seem to support conventional s-wave superconductivity in BiS_2-based compounds, the exotic superconducting properties of some of the BiS_2-based compounds are still under debate. A typical example is the coexistence of superconductivity and ferromagnetism for $CeO_{1-x}F_xBiS_2$ [10, 71]. Systematic studies on the system $CeO_{1-x}F_xBiS_2$ ($0 \le x \le 0.9$) suggest that ferromagnetism and superconductivity develop simultaneously with increasing F concentration, even though the sign of Θ_{CW} is negative. Two ferromagnetic phases with respective Curie temperatures of 4.5 K and 7.5 K are induced with increasing F concentration. This result indicates that charge carriers, generated by F substitution, are introduced into the blocking CeO layers in addition to the superconducting BiS_2 layers [81, 71].

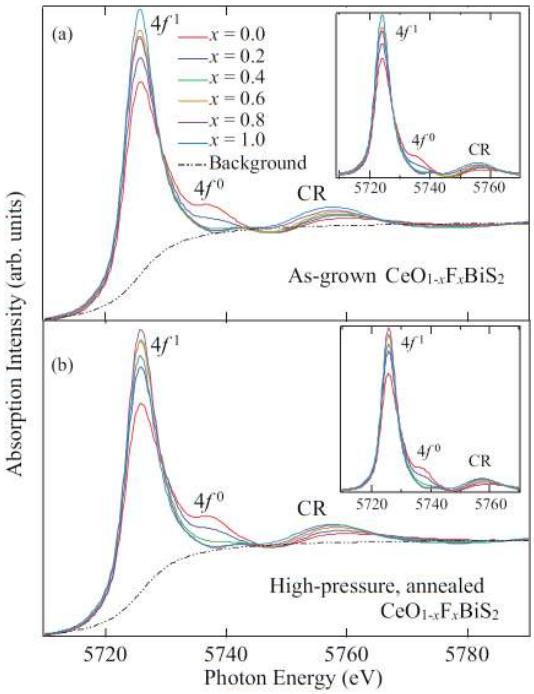

Figure 14: (Color online) Ce L_3-edge normalized x-ray absorption spectroscopy data of as-grown and (b) high-pressure annealed samples of $CeO_{1-x}F_xBiS_2$ with $x = 0$, 0.2, 0.4, 0.6, 0.8, and 1.0. The $4f^1$, $4f^0$, and continuum resonance peaks around 5725, 5737, and 5758 eV are shown. The background (arctangent function) subtracted spectra are shown in the insets. The spectra were taken at room temperature in transmission mode (after Sugimoto *et al.* [44]).

In addition, ferromagnetism and superconductivity are both enhanced in the samples synthesized by HP annealing, indicating sensitivity of these states to local atomic displacements.

Ce L_3 x-ray absorption spectroscopy (XAS) is a direct probe of the local structure around a selected absorbing atom and the distribution of valence electrons, with the final states in the continuum being due to multiple scattering resonances of the photoelectrons in a finite cluster [44]. Ce L_3 XAS was used to investigate the effect of F substitution on the local electronic and lattice structures of the system $CeO_{1-x}F_xBiS_2$ in as grown (AG) and HP annealed samples [44]. Since it is difficult to prepare clean surfaces using the available polycrystalline samples, bulk-sensitive Ce L_3-edge XAS measurements taken in the transmission mode are the most reliable tool to evaluate the Ce valence.

The Ce L_3-edge XAS spectra of AG and HP annealed samples of $CeO_{1-x}F_xBiS_2$ (x = 0, 0.2, 0.4, 0.6, 0.8, and 1.0) are shown in Figs. 14(a) and (b), respectively [44]. The spectra are normalized with respect to the atomic absorption estimated by a linear fit to the high energy part of the spectra. Three salient structures around 5725, 5737, and 5758 eV can be identified within the Ce L_3-edge XAS spectrum. The first peak near 5725 eV is the absorption white line corresponding to the transition from the Ce $2p$ core level to the vacant Ce $5d$ state mixed with the Ce $4f^1$ final state [44]. The second peak near 5737 eV corresponds to the transition from the Ce $2p$ core level to the vacant Ce $5d$ state mixed with the Ce $4f^1$ final state. The $4f^1$ and $4f^0$ final states are the so-called well-screened and poorly-screened states, respectively, and provide information concerning the Ce valence. The presence of both $4f^1$ and $4f^0$ states suggests Ce^{3+}/Ce^{4+} valence fluctuations. The energy difference between the $4f^1$ and $4f^0$ absorption peaks, approximately 12 eV [44], is mainly determined by the Ce $2p$-Ce $4f$ Coulomb interaction and is expected to be independent of the F concentration. There is a systematic change due to F substitution in the $4f^1$ and $4f^0$ peak intensities as seen Figs. 14(a) and (b). The third peak near 5758 eV provides the information on the local lattice structure. This peak is the so-called continuum resonance (CR), likely due to Ce-Bi scattering with a contribution from the Ce-Ce scattering and reflecting the evolution of the Ce-Bi/Ce bond length. In addition, there is a weak feature near 5742 eV. This feature is a characteristic of layered rare-earth systems, and its intensity is generally sensitive to the O/F atom disorder in the CeO/F layer. On the other hand, the calculated relative spectral weight $4f^0/[4f^1 + 4f^0]$ for both AG and HP annealed $CeO_{1-x}F_xBiS_2$ samples indicates that the Ce^{4+} state with the $4f^0$ electronic configuration in $CeOBiS_2$, coexists with the Ce^{3+} state with $4f^1$ electronic configuration [44]. This result confirms the presence of valence fluctuations in $CeOBiS_2$ between the Ce^{3+} and Ce^{4+} electronic configurations. The $4f^0/[4f^1 + 4f^0]$ value decreases with increasing F concentration both in the AG and HP samples. The small difference in $4f^0/[4f^1 + 4f^0]$ between the AG and HP annealed samples indicates that there are some additional factors, such as sample inhomogeneity, that play an important role in controlling the valence of Ce.

The layered crystal structure of $CeOBiS_2$ is displayed in Fig. 15, which contains BiS_2 layers intercalated with a CeO layer. The in-plane S atoms in the BiS_2 layer [labeled S1 in Fig. 15(a)] are located a distance of ~2.8 Å from the Bi atoms, while the out-of-plane S [labeled S2 in Fig. 15(a)] atoms linking the spacer layer with the BiS_2 plane are located a distance of ~2.6 Å from the Bi atoms. With F substitution, the Bi-S2 distance increases (ΔR_{max} ~ 0.12 Å), while the Ce-S2 distance decreases (ΔR_{max} ~ 0.15 Å), leading to a disruption of the Ce-S-Bi coupling channel as depicted in Figs. 15(b) and (c). Consequently, the hybridization between the Ce $4f$ orbital and the Bi $6p$ conduction band decreases with F substitution and the Ce^{3+}/Ce^{4+} valence fluctuation is suppressed. This means that F substitution drives the system from the Ce^{3+}/Ce^{4+} valence fluctuation regime to the Ce^{3+} Kondo-like regime [82]. Indeed, the Ce $4f^0$ spectral weight almost disappears for $x > 0.4$, where the system exhibits coexistence between superconductivity and ferromagnetism at low temperature. Therefore, it seems that the mixed valence of Ce, driven by the coupling between the Ce $4f$ and Bi $6p$ electron states, disrupts superconductivity. The Ce $4f$ electrons are localized in the Kondo regime for $x > 0.4$ and favor ferromagnetic polarization of the localized magnetic moments. The direct Ce-Ce exchange interaction plays an important role in the ferromagnetic order observed in many Ce compounds [83, 84, 85, 86]. In $CeO_{1-x}F_xBiS_2$, the Ce-Ce distance is larger than that of most ferromagnetic Ce compounds. Therefore, rather than the direct Ce-Ce exchange interaction, a Ce-S-Ce superexchange interaction between Ce^{3+} sites as depicted in Figs. 15(c) is expected to be responsible for ferromagnetism in the $CeO_{1-x}F_x$ layer. For $x > 0.4$, the ferromagnetic $CeO_{1-x}F_x$

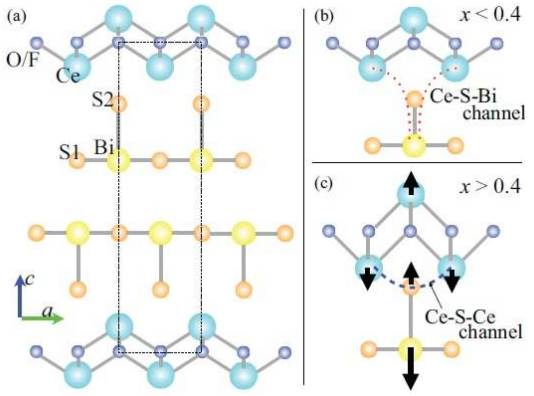

Figure 15: (Color online) The crystal structure of $CeO_{1-x}F_xBiS_2$. The dashed box represents the unit cell. (b) The local structure of $CeO_{1-x}F_xBiS_2$ for $x < 0.4$ and (c) for $x > 0.4$. The Ce-S2 bond length decreases while the Bi-S2 bond length increases when $x > 0.4$ (after Sugimoto *et al*. [44]).

layer is expected to be insulating just like the $LaO_{1-x}F_x$ layer, and is decoupled from the superconducting BiS_2 layer.

Coexistence between superconductivity and ferromagnetism is also observed in Ce-substituted $Sr_{0.5}Ce_{0.5}FBiS_2$ [72]. It has been reported that superconductivity can be induced with T_c near 3 K, and that the dilute Ce lattice orders ferromagnetically below 7.5 K with only 50% Ce concentration in the (Sr,Ce)F layer [72]. Generally, superconductivity competes with magnetic order; however, for the systems $CeO_{1-x}F_xBiS_2$ and $Sr_{0.5}Ce_{0.5}FBiS_2$, the ferromagnetic transition temperatures are substantially higher than T_c. On the other hand, Ce substitution introduces charge carriers that induce superconductivity in addition to the ferromagnetic order, implying that the interaction between the Ce $4f$ electrons and conduction electrons may be anisotropic. Thus, there may be an intrinsic coexistence of ferromagnetism and superconductivity, and each can be induced by Ce substitution.

10. Anisotropic upper critical fields H_{c2}

The BiS_2-based superconductors are found to be type-II superconductors. The superconducting states can be destroyed by relatively small applied magnetic fields of $\mu_0 H \approx 1$ T for polycrystalline samples [8]. The magnetic-field dependence of the electrical resistivity in a pulse magnetic field up to ~56 T for a $LaO_{0.5}F_{0.5}BiS_2$ polycrystalline sample, which was prepared using the HP synthesis method, was measured by Mizuguchi *et al*. [88]. Figure 16(a) displays the $d\rho/dT$ vs. T and ρ vs. T data for $LaO_{0.5}F_{0.5}BiS_2$ under an applied magnetic field of $\mu_0 H = 8$ T. One can see that the temperature of the onset superconductivity T^{max} is still near 9 K. T_c^{onset} is defined as the temperature at which $d\rho/dT = 0$. The inflection point, T^{mid}, appears at $T \sim 5.3$ K at which the value of $d\rho/dT$ begins to increase and the electrical resistivity decreases. This indicates that the evolution of the superconducting current path is below T^{mid}. With increasing magnetic field, the anomaly at T^{mid} becomes more pronounced and overlaps with T_c^{onset} as is presented in Fig. 16(b). The evolution of the superconducting current path corresponds to T^{max} under lower magnetic fields and to T^{mid} under higher magnetic fields. Figure 16(b) also indicates the temperature dependence of the upper critical field, which changes slope at an applied magnetic field of $\mu_0 H = 8$ T. This behavior was explained by defining three distinct upper critical fields, $\mu_0 H_{c2}^{max}$, $\mu_0 H_{c2}^{mid}$, and $\mu_0 H_{c2}^{min}$. The lowest upper critical field, $\mu_0 H_{c2}^{min}$, is regarded as the magnetic field where the superconducting states of grains with an orientation of $H \| c$ are suppressed. The middle, $\mu_0 H_{c2}^{mid}$, and maximum, $\mu_0 H_{c2}^{max}$, upper critical fields are regarded as the magnetic fields where the superconducting states of the grains with an orientation of $H \| ab$ are suppressed. As is shown in Fig. 16(b), $\mu_0 H_{c2}^{min}$ is lower than $\mu_0 H_{c2}^{mid}$, and $\mu_0 H_{c2}^{max}$, which indicates that the upper critical fields of $LaO_{0.5}F_{0.5}BiS_2$ are anisotropic. A smaller value of $\mu_0 H_{c2}^{min}$ compared to $\mu_0 H_{c2}^{mid}$ and $\mu_0 H_{c2}^{max}$ indicates that the superconducting current path can easily be suppressed under magnetic fields for grains with an orientation of $H \| c$. The difference between $\mu_0 H_{c2}^{mid}$ and $\mu_0 H_{c2}^{max}$ might be related to the anisotropy of the superconducting states within the Bi-S plane, which might be caused by a structural distortion induced by the HP synthesis technique. If the *ab* plane is distorted, the superconducting state along the *a*-axis could be nonequivalent to that along the *b* axis which could cause differences in the upper critical field and anisotropic effective masses. The upper critical fields for $LaO_{0.5}F_{0.5}BiS_2$ $\mu_0 H_{c2}^{max}(T)$, $\mu_0 H_{c2}^{mid}(T)$, and $\mu_0 H_{c2}^{min}(T)$ are plotted in Fig. 16(c) and exhibit significant anisotropy. The estimated initial slopes of the upper critical fields, $d\mu_0 H_{c2}^{max}/dT$, $d\mu_0 H_{c2}^{mid}/dT$, and $d\mu_0 H_{c2}^{min}/dT$ were determined by fitting a line to the data. The values obtained by this analysis are -7.05, -2.60, and -0.95 T/K, respectively, which yield an estimated anisotropy parameter for the critical field of ~7.4 for $LaO_{0.5}F_{0.5}BiS_2$ using the values of $d\mu_0 H_{c2}^{max}/dT$ and $d\mu_0 H_{c2}^{min}/dT$ [88].

We also consider measurements of the upper critical field H_{c2} for $NdO_{0.5}F_{0.5}BiS_2$ samples in single-crystalline form, which provide definitive information concerning the superconducting anisotropy at low temperatures as well as its temperature dependence [26, 28, 27]. Electrical resistivity $\rho(T)$ data for a $NdO_{1-x}F_xBiS_2$ single crystal at ambient magnetic field and under applied magnetic fields with $H \| c$-axis$\perp I$, $H \| I \| a$-axis (the current is applied along the *a*-axis) are displayed in Figs. 17(a) and (b). Electrical resistivity decreases slightly with decreasing temperature down to 6 K, which indicates that the behavior is metallic, in contrast to the semiconducting behavior of polycrystalline samples [8, 10, 89]. We assume that the intrinsic transport behavior of the $NdO_{1-x}F_xBiS_2$ single crystal is metallic, and that the transport behavior of the polycrystalline sample is semiconducting due to the existence of grain boundaries. In the inset of Fig. 17(a), ZFC and FC measurements of DC magnetic susceptibility, χ, in $H = 1$ Oe for $NdO_{0.5}F_{0.5}BiS_2$ exhibit diamagnetic screening signals with a T_c onset value that is consistent with the $\rho(T)$ data [26]. As is presented in Fig. 17(a), superconductivity is suppressed down to 2 K with a magnetic field of only 0.6 T, applied with H ||*c*-axis. However, superconductivity is very robust when H ||*a*-axis and is still observed above 2 K when the magnetic field is as high as 9 T.

One can clearly see an enhanced excess conductivity above T_c if the electrical resistivity curve between 20-30 K is ex-

Table 2: Summary of magnetic and thermodynamic properties for selected BiS_2-based compounds. Included in the table are Curie-Weiss temperature Θ_{CW}; effective magnetic moment μ_{eff}; magnetic ordering temperature T_C or T_N; Debye temperature Θ_D; the Sommerfeld coefficient of the specific heat, γ; jump in the specific heat at T_c normalized by γT_c, $\Delta C/\gamma T_c$; references from which table entries are obtained.

Compound	Θ_{CW}, (K)	μ_{eff}, (μ_B)	T_C or T_N, (K)	Θ_D, (K)	γ, ($\frac{mJ}{mol-K^2}$)	$\Delta C/\gamma T_c$	References
$Bi_4O_4S_3$	–	0.096	–	192	2.8	1.43	[40]
$LaO_{0.5}F_{0.5}BiS_2$	–	–	–	221	2.53	0.94	[8]
$CeO_{0.5}F_{0.5}BiS_2$	-8.38	2.62	~5	224	58.1	–	[8]
$PrO_{0.5}F_{0.5}BiS_2$	-23.71	3.49	–	209	58	–	[8]
$NdO_{0.5}F_{0.5}BiS_2$	-6.57	3.46	–	190	26.2	–	[8, 49]
$YbO_{0.5}F_{0.5}BiS_2$	-5.43	4.42	~2.7	186	30.1	–	[8]
$EuBiS_2F$	–	7.2	–	201	73.3	–	[52]
$La_{0.75}Y_{0.25}O_{0.5}F_{0.5}BiS_2$	–	–	–	227	2.21	0.9	[78]
$La_{0.85}Th_{0.15}O_{0.5}F_{0.5}BiS_2$	–	–	–	220	0.58	0.91	[11]
$Sr_{0.55}La_{0.45}FBiS_2$	–	–	–	190	1.6	1.1	[87, 50]

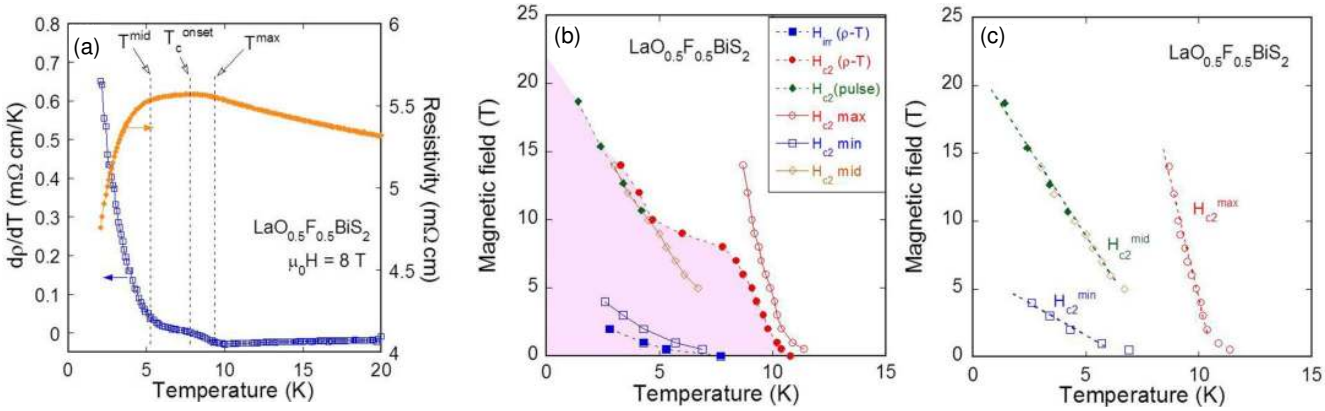

Figure 16: (Color online) (a) Electrical resistivity ρ (right axis) and $d\rho/dT$ (left axis) vs. temperature T for $LaO_{0.5}F_{0.5}BiS_2$, measured in an applied magnetic field $\mu_0 H = 8$ T. Temperatures in the vicinity of the superconducting transition T^{max}, T_c^{onset}, and T^{mid} (defined in the text) are indicated by arrows and dashed lines. (b) The $\mu_0 H - T$ phase diagram for $LaO_{0.5}F_{0.5}BiS_2$. Upper critical field curves $\mu_0 H_{c2}(T)$ are estimated from measurements of a polycrystalline sample using various criteria and are displayed as $\mu_0 H_{c2}(\rho - T)$, $\mu_0 H_{c2}$ (pulse), $\mu_0 H_{c2}$ max, $\mu_0 H_{c2}$ min, and $\mu_0 H_{c2}$ mid (defined in the text). The values of $\mu_0 H_{irr}(\rho - T)$ are also displayed. The colored area is bounded by the $H_{c2}(T)$ curves obtained from measurements in a pulsed magnetic field and at lower fields. The other curves are obtained from observing the evolution of various features in $\rho(T)$ data. These features probably indicate that certain grains in the polycrystalline sample enter the normal state at different fields, suggesting that $H_{c2}(T)$ curves for $LaO_{0.5}F_{0.5}BiS_2$ are anisotropic. (c) The curves $\mu_0 H_{c2}$ max, $\mu_0 H_{c2}$ min, and $\mu_0 H_{c2}$ mid from panel (b) are displayed. Dashed lines are linear fits to each curve that are used to estimate initial temperature derivatives $d\mu_0 H_{c2}/dT$ for each curve (after Mizuguchi *et al.* [88]).

trapolated linearly to low temperatures. This suggests a giant superconducting fluctuation effect in the $NdO_{1-x}F_xBiS_2$ single crystals. To illustrate this, the difference between the measured electrical resistivity data ($\rho = 1/\sigma$) and the extrapolated line ($\rho_n = 1/\sigma_n$), $\Delta\rho = \rho_n - \rho = 1/\sigma_n - 1/\sigma = \Delta\sigma/\sigma\sigma_n$, where σ, σ_n, and $\Delta\sigma$ are the measured, extrapolated, and the excess conductivities, respectively, is presented in the inset of Fig. 17(b). It is clear that $\Delta\rho$ vanishes near 15 K. In Fig. 17(c), the $\rho(T)$ curve from another sample indicates that the superconducting fluctuating region extends up to about 20 K, as marked by T^*. In order to check whether or not there are strong superconducting fluctuations, the in-plane electrical resistivity with a rotating in-plane magnetic field has been measured on a $NdO_{1-x}F_xBiS_2$ single crystal [26]. The current is applied along the a- (or b-) axis, and the sample is rotated with an in-plane magnetic field. The angle enclosed between the current direction and the magnetic field is ϕ. When $\phi = 0 = \pi$, the Lorentz force on the vortices is zero and the dissipation is at a minimum. Dissipation is maximized when $\phi = \pi/2 = 3\pi/2$. Interestingly, the same two-fold oscillations appear from 4 K all the way up to 10 K. At 4 K, the vortex motion dominates the dissipation. From the systematic evolution observed from 4 to 10 K, the two-fold resistivity oscillation is still induced by the vortex motion, even at 10 K. This leads to the conclusion that the superconducting fluctuations exist up to at least 10 K from the angle-dependent resistivity data; though, the bulk transition occurs at $T_c = 5$ K.

Another interesting phenomenon is that the normal-state behavior is semiconducting-like when superconductivity is completely suppressed as is shown in Fig. 17(a). Similar behavior was observed and emphasized in polycrystalline $CeO_{1-x}F_xBiS_2$ samples [71, 15]. This is counterintuitive and contrary to the BCS picture, since a metallic state should be recovered in the normal state. One may argue that this semiconducting behavior is induced by a localization effect of electrons in a low-dimensional system as derived from the band structure calculations [21, 58]. This scheme is, however, also impractical; for a low-dimensional system, impurities may induce semiconducting behavior due to localization, but the magnetic field will weaken this localization effect and the semiconducting behavior to which it leads. In our case, when superconductivity is suppressed, the semiconducting feature above T_c emerges. Furthermore, the magnetic field seems to promote this semiconducting behavior in a certain field region. Therefore, this semiconducting feature of the normal state under a magnetic field is non-trivial and requires further investigation.

In one study of $NdO_{0.5}F_{0.5}BiS_2$ single crystals, distinct T_c's were defined by the temperatures where $\rho(T)$ data reach values of 50%, 90%, and 98% of the normal state value ρ_n, determined by linearly extrapolating the electrical resistivity data between 20-30 K to low temperature. The upper critical fields, $H_{c2}(T)$, were estimated using these three criteria for determining T_c and are presented in Fig. 17(d) [26]. The $H_{c2}(T)$ curves determined by the above three criteria are quite different for the cases of $H||c\perp I$ and $H||I||a$. The anisotropy, characterized by the relation $\gamma' = [dH^{ab}_{c2}(T)/dT]/[dH^{c}_{c2}(T)/dT]$ near T_c, is found to be roughly 30-45, which is an order of magnitude larger than $\gamma' \sim 7.4$ for $LaO_{0.5}F_{0.5}BiS_2$ [88]. The Werthamer-

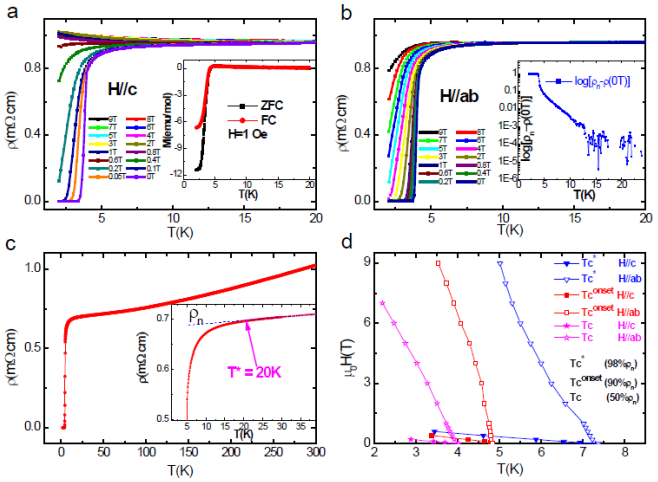

Figure 17: (Color online) Electrical resistivity, magnetic susceptibility, and upper critical field of $NdO_{0.5}F_{0.5}BiS_2$. (a, b) The temperature dependence of electrical resistivity for a $NdO_{0.5}F_{0.5}BiS_2$ single crystal at zero field and under magnetic fields $H||c$ (a) and $H||ab$ (b) up to 9 T. The inset of (a) shows the zero-field-cooled (ZFC) and field-cooled (FC) magnetic susceptibility data at 1 Oe. The inset of (b) shows the temperature dependence of $\log\rho = \log[\rho_n - \rho(0\ \mathrm{T})]$. (c) The temperature dependence of electrical resistivity for a $NdO_{0.5}F_{0.5}BiS_2$ single crystal at zero field from 2 K to 300 K; the inset displays evidence for superconducting fluctuations up to 20 K. (d) the upper critical field determined using the criteria of T_c defined by 98%ρ_n, 90%ρ_n, and 50%ρ_n with $H||c$ and $H||ab$ where ρ_n is the normal-state electrical resistivity (after Liu *et al.* [26]).

Helfand-Hohenberg (WHH) formula [90] is also used to estimate the orbital upper critical field $H^*_{c2}(T)$ at zero temperature where $H^*_{c2} = -0.69T_c[dH_{c2}/dT]_{T_c}$. If we consider the $H_{c2}(T)$ data for which T_c was defined by the temperature where $\rho(T)$ decreases to 90% of ρ_n, we obtain the following relevant parameters: $T_c = 4.83$ K (in zero magnetic field), and $[dH^{ab}_{c2}(T)/dT]$ = -12 T/K and $[dH^{c}_{c2}(T)/dT]$ = -0.25 T/K near T_c. Using the WHH formula, orbital upper critical fields of $H^{*,ab}_{c2}(0) = 40$ T and $H^{*,c}_{c2}(0) = 0.833$ T are estimated. This huge anisotropy has only been observed in the Bi-based cuprates, suggesting that Josephson vortices are certainly expected in these new BiS_2-based superconducting systems [26, 28].

There is an uncertainty associated with determining the anisotropy (γ') by the procedure described above because, (1) the upper critical field is dependent on the criterion used to define T_c and, (2) the $H^{ab,c}_{c2}(T)$ curves are not linear near T_c. According to the anisotropic Ginzburg-Landau theory, the electrical resistivity in the mixed state depends on the effective magnetic field $H/H^{GL}_{c2}(\theta)$ with the angle, θ, subtending the c-axis and the magnetic field direction. The effective upper critical field $H^{GL}_{c2}(\theta)$ at an angle θ is given by: $H^{GL}_{c2}(\theta) = H^{c}_{c2}/\sqrt{\cos^2(\theta) + \gamma'^{-2}\sin^2(\theta)}$. Therefore, by using a dimensionless scaling variable, $H/H^{GL}_{c2}(\theta) = H\sqrt{\cos^2(\theta) + \gamma'^{-2}\sin^2(\theta)}$, the electrical resistivity measured at different magnetic fields with a fixed temperature should collapse onto a single curve [91]. In Figs. 18(a), (b), and (c), the angular dependence of the in-plane electrical resistivity at 3, 3.5 and 4 K is displayed, where the applied current flows along the a-axis and the magnetic field is applied perpendicular to the current direction.

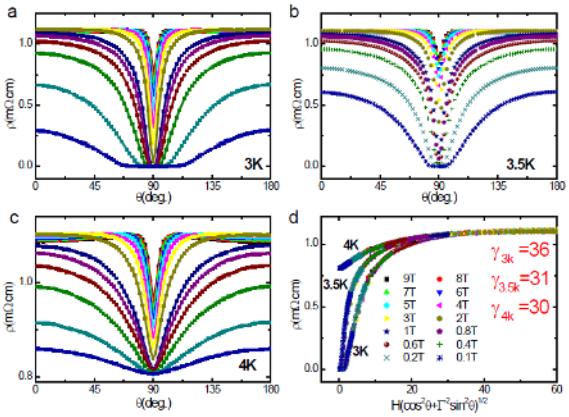

Figure 18: (Color online) Angular dependence of electrical resistivity and anisotropy for a $NdO_{0.5}F_{0.5}BiS_2$ single crystal. (a, b, c) Angular dependence of electrical resistivity at (a) 3 K, (b) 3.5 K, and (c) 4 K with $\mu_0 H$ from 0.1 T to 9 T. Here, θ is the angle between the magnetic field and the c-axis, with current flowing in-plane and perpendicular to the field. (d) Scaling of the electrical resistivity vs. $H/H_{c2}^{GL}(\theta) = H\sqrt{\cos^2(\theta) + \gamma'^{-2}\sin^2(\theta)}$ at 3, 3.5 and 4 K in different magnetic fields. The data measured at a fixed temperature and different magnetic fields are scaled well by adjusting γ' (after Liu *et al.* [26]).

Fig. 18(d) presents the scaling that is obtained by the above-mentioned method. The scaling is excellent over a wide range of $H/H_{c2}^{GL}(\theta)$ for all three temperatures, yielding anisotropies of 36, 31, and 30, respectively. Therefore, it can be concluded that the anisotropy of $NdO_{0.5}F_{0.5}BiS_2$ is about 30-45.

11. Magnetic penetration depth

The magnetic penetration depth as a function of temperature $\lambda(T)$ is a useful parameter for probing the superconducting order parameter and establishing the pairing symmetry. In the conventional BCS theory, the Cooper pairs consist of two electrons with opposite momenta and spins, and the pairing is mediated by phonons. The ratio of the superconducting gap to the superconducting transition temperature is predicted to be $2\Delta/k_BT_c = 3.53$ in the weak coupling limit. Penetration depth measurements are directly proportional to the superfluid density, $\rho \propto 1/\lambda^2$, and therefore to the magnitude of the superconducting order parameter $\Delta(T)$, which is the superconducting energy gap for quasi-particle excitations in the superconducting ground state. $\lambda(T)$ is an important parameter that is used to distinguish between different possible superconducting energy gap structures and to help identify the superconducting pairing mechanism.

$\lambda(T)$ was measured in $Bi_4O_4S_3$ by μSR measurements[30] and using tunnel-diode-oscillator technique[32]. The superfluid density ρ, determined from these measurements, was found to be very low. The temperature dependence of λ^{-2} possibly suggests the presence of two s-wave type energy gaps with zero-temperature values of $\Delta_1(0) = 0.93(3)$ and $\Delta_2(0) = 0.09(4)$ meV. The presence of two superconducting energy gaps is consistent with band-structure calculations that suggest two bands cross the Fermi level, the RPA analysis of a two-orbital model for the BiS_2-based superconductors [21, 63], and other experimental studies involving Hall effect, Seebeck coefficient, and magnetoresistance measurements [31, 32, 34]. However, a single-gap s-wave model fit with a gap of 0.88(2) meV cannot be ruled out completely. The value of $\lambda(T)$ at $T = 0$ K is estimated to be $\lambda(0) = 861(17)$ nm, which is one of the largest values among all known layered superconductors. This reflects a very low superfluid density. In $Bi_4O_4S_3$ polycrystalline samples, penetration-depth measurements based on the tunnel-diode-oscillator technique revealed a single gap with $2\Delta_s/k_BT_c = 7.2$, indicating the existence of strong electron-phonon coupling in $Bi_4O_4S_3$ [32]. On the other hand, measurements of μSR provide possible evidence for multiple gaps with $2\Delta_s^1/k_BT_c = 5.92$ and $2\Delta_s^2/k_BT_c = 0.86$ [30].

$\lambda(T)$ measurements were also performed on $LaO_{0.5}F_{0.5}BiS_2$, $LaO_{0.5}F_{0.5}BiSe_2$, and $NdO_{1-x}F_xBiS_2$ ($x = 0.3$, 0.5) superconductors. These measurements yielded superfluid densities with temperature dependencies that are consistent with the s-wave character; the $2\Delta/k_BT_c$ values are very close to that expected for phonon-mediated pairing [92, 38, 12]. We note, however, that these penetration depth studies are unable to rule out the possibility of an anisotropic gap symmetry. The high value of the Ginzburg-Landau parameter $\kappa(0) = \lambda_{ab}/\xi \simeq 85$ for $LaO_{0.5}F_{0.5}BiS_2$, where $\xi(0) = [\phi_0/2\pi H_{c2}(0)]^{1/2} \approx 5.3$ nm is the zero-temperature limit of the coherence length extracted from the upper critical field [55, 42], places this compound in the extreme type-II superconductor limit. Finally, the in-plane magnetic penetration depth, $\lambda_{ab}(1.7\text{ K}) = 484 \pm 3$ nm, for $LaO_{0.5}F_{0.5}BiS_2$ indicates a very dilute superfluid density, typical of systems with a nearly 2D character [38]. Similar large magnetic penetration depth values are observed for $LaO_{0.5}F_{0.5}BiSe_2$ and $NdO_{1-x}F_xBiS_2$ ($x = 0.3$, 0.5) [12, 92].

12. Electron tunneling measurements

Another powerful technique to address the pairing symmetries is scanning tunneling spectroscopy (STS) using a scanning tunneling microscope (STM). This probe has been used to determine the pairing symmetries in a large variety of superconductors. Additionally, this technique has made significant contributions through its ability to visualize CDW order and other electronic ordered states, and to disentangle the relationships between superconductivity and such states [48].

From the measured tunneling spectra for $Bi_4O_4S_3$ [31], a superconducting energy gap of about 3 meV, and corresponding ratio $2\Delta/k_BT_c \sim 16.6$ has been observed. This ratio is larger than the value determined from μSR measurements [30]. It is even larger than the values observed for most high-T_c superconductors [2, 3, 4, 5]. The gapped feature in the STS vanishes at $T \approx 14$ K, which is much higher than the T_c for bulk superconductivity. A similar feature has been attributed to a pseudogap in the cuprates [93]. However, transport data do not provide any evidence for a pseudogap, indicating that the gapped feature in STS measurements might instead be related to superconducting fluctuations. If one uses $T_f = 14$ K as the pairing temperature, $2\Delta/k_BT_f \sim 5$, which is still a large value, but comparable to the value determined from μSR measurements. This is indicative of strong coupling superconductivity in the $Bi_4O_4S_3$ compound.

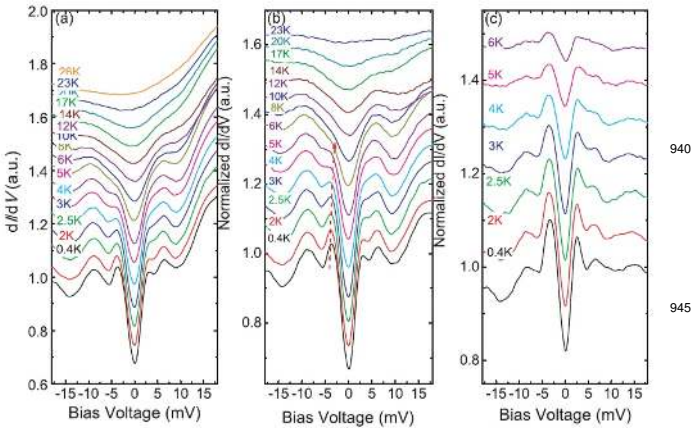

Figure 19: (Color online) The evolution of scanning tunneling spectroscopy (STS) with temperatures from 0.4 K to 26 K for Nd(O, F)BiS_2 single crystals. The STS spectra are offset for clarity. In the low-temperature region, the superconducting coherence peaks emerge at about ±3.5(±0.3) meV and two higher-energy hump features arise near ±7.5(±1) meV. (b) The STS spectra, normalized by the spectrum measured at 26 K. A dashed red line highlights the superconducting coherence peaks at around 3.5 meV. (c) The STS spectra, normalized by the one measured at 8 K (after Liu *et al*. [26]).

Because of strong scattering in the polycrystalline sample, it is very difficult to estimate the pairing symmetry from fits to the μSR spectra.

From STS data measured at temperatures between 0.4 K and 26 K for Nd(O,F)BiS_2 [48, 26], two gap features at different energies are shown in Fig. 19. The smaller gap $\Delta_s^1 \approx 3.5 \pm 0.3$ meV corresponds to the bulk transition at $T_c = 4.83$ K, thus the ratio is $2\Delta_s^1/k_BT_c = 16.8$. This is much larger than the theoretical value of 3.5 in the weak-coupling limit of the BCS model and is inconsistent with the μSR measurements [92, 38]. If the upper boundary of the superconducting fluctuation temperature of ∼ 20 K is used as the pairing temperature, a value $2\Delta_s^1/k_BT_c = 4.06$ is obtained, which is not far from the BCS value of 3.5. If this interpretation is correct, it could be inferred that the superconducting pairing occurs at a high temperature (near 20 K), leading to strong superconducting fluctuations. This scenario is also supported by the electrical transport measurements discussed above [26]. This situation resembles the case in cuprate superconductors. Furthermore, the energy gap feature at $2\Delta_s^2/k_BT_c \approx 7.5 \pm 1$ meV (where the superscript 2 indicates that this gap is distinct from Δ_s^1 and should not be confused with a gap squared) may be a pseudogap, induced by the tendency toward CDW order or by local pairing governed by the valence fluctuations of the Bi ionic state. A picture involving competing order and superconductivity appears to be quite general in the cuprates, iron pnictide/chalcogenides, and the BiS_2-based compounds. On the other hand, if superconductivity is induced by the correlation effect and there are enhanced ferromagnetic-like spin fluctuations, a spin-triplet pairing state could also be possible. However, evidence is still lacking for spin-triplet pairing has not yet been observed in the BiS_2-based superconductors.

13. Optical spectroscopy

Optical spectroscopy measurements performed on Nd(O,F)BiS_2 single crystals reveal a simple metallic response with a relatively low screened plasma edge near 5000 cm^{-1} [22]. The plasma frequency is estimated to be 2.1 eV, which is much smaller than the value expected from first-principles calculations for an electron doping level of $x = 0.5$, but very close to the value based on a doping level of 7% itinerant electrons per Bi site as determined by ARPES experiments [74, 80]. The energy scales of the interband transitions are also well reproduced by first-principles calculations [20, 58, 40]. Usually, the ratio of experimental kinetic energy K_{exp} to the theoretical kinetic energy K_{band} from density-functional theory calculations provides a measure of the degree of correlations [94]. The kinetic energy is proportional to the spectral weight $\omega_p^2/8$, defined as the area under the Drude part of $\sigma_1(\omega)$. The extremely close values of the plasma frequencies, determined by both experiment and generalized gradient approximation (GGA) calculations, implies $K_{exp}/K_{band} = \omega_{p,exp}^2/\omega_{p,band}^2 \approx 1$, suggesting that Nd(O,F)BiS_2 is a simple metal and correlation effects are almost completely absent. This result is consistent with recent ARPES measurements [74, 80]. The absence of electronic correlation effects and the surprisingly good agreement between experimental optical spectroscopy measurements and first-principles calculations suggest that the BiS_2-based compounds are ordinary metals. Furthermore, any scenario involving exotic pairing mechanisms or strong electronic correlation effects appears to be unjustified. The small plasma frequency, which is in good agreement with the small Fermi surfaces observed from ARPES measurements, suggests that Nd(O,F)BiS_2 is far from a CDW instability near $x = 0.5$, as proposed in early theoretical calculations. As proposed in early work [74, 80], subnominal F concentrations could be due to facilitated by Bi vacancies in the samples.

Qazilbash *et al*. have described a quantitative and intuitive systematic classification of the degree of conduction-electron correlations in a wide variety of materials ranging from Mott insulators to free-electron metals, including the Fe-based pnictides LaFePO and $BaFe_2As_2$. This classification system is based on the ratio of the experimentally-determined optical spectral weight of the conduction-carrier conductivity (the low-frequency Drude contribution K_{exp}) to that predicted by band theory (K_{band}) [94]. For example, the strongly-correlated, integer-valent, layered cuprate parent compound La_2CuO_4 is predicted by conventional band theory to be a good metal, but is instead an electrical insulator due to Coulomb (Mott-Hubbard) electronic correlations. Therefore, it does not have a Drude peak in the real part of the optical conductivity [94], giving $K_{exp}/K_{band} = 0$. One would expect K_{exp}/K_{band} to decrease as the degree of electronic correlations increases, with $0 \leq K_{exp}/K_{band} \leq 1$. Qazilbash *et al*. found $K_{exp}/K_{band} \approx 0.5$ and 0.3 for LaFePO and $BaFe_2As_2$, respectively, and compared these values with corresponding data for a wide variety of other compounds with varying degrees of electronic correlations as shown in Fig. 20 [94]. The FeAs-based materials are found from this analysis to have an intermediate level of electronic correlations and

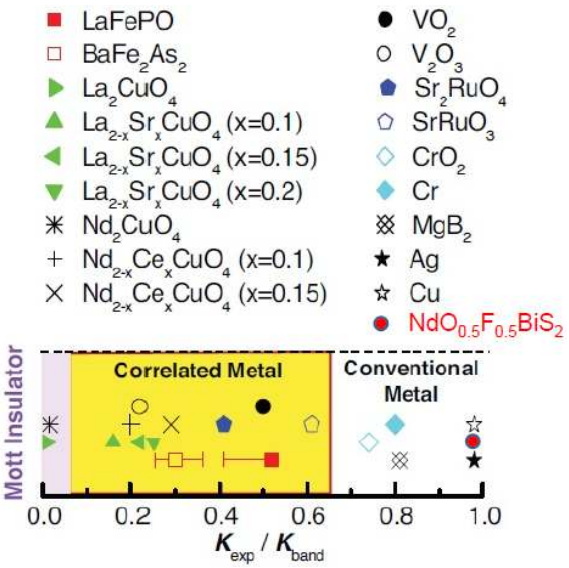

Figure 20: (Color online) Ratio of the experimental conduction carrier optical spectral weight (expressed as a kinetic energy) K_{exp} to that calculated value using band theory (K_{band}) for a variety of materials. This ratio is the square of the ratio of the experimental to the theoretical band plasma frequency. The degree of conduction electron correlations in a material corresponds to how far K_{exp}/K_{band} is from unity. Mott-Hubbard insulators are on the far left and have ratios close to zero because the measured conduction carrier density, and therefore the plasma frequency, are close to zero, whereas band theory predicts that they are metals. At the opposite extreme, conventional free-electron metals like Cu and Ag are on the far right and have ratios close to unity. According to this scheme, Nd(O,F)BiS_2 is a conventional metal like the elements Cu and Ag (after Qazilbash *et al.* [94] and Wang *et al.* [22]).

Nd(O,F)BiS_2 is located on the conventional metal side of the continuum along with the elements Ag and Cu.

14. Superconducting properties under pressure

The evolution of T_c under applied pressures up to 1.92 GPa for the compound $Bi_4O_4S_3$ was investigated by Kotegawa *et al.* [15]. It was found that T_c decreases monotonically without a distinct change in the metallic behavior in the normal state [15]. The temperature dependence of the electrical resistivity ρ and the evolution of T_c under applied pressure for $LnO_{0.5}F_{0.5}BiS_2$ samples were reported by Wolowiec *et al*[17, 18, 19] and Tomita *et al*[19]. As shown in the phase diagrams in Fig. 21, each of the four compounds $LnO_{0.5}F_{0.5}BiS_2$ (Ln = La, Ce, Pr, Nd) exhibits an abrupt pressure-induced transition from a low T_c superconducting phase at lower pressure to a high T_c superconducting phase at higher pressure. In the four compounds, the pressure-induced transition observed in the superconducting state is coincident with changes in the suppression of ρ in the normal state. The rate of suppression of semiconducting behavior and the rate of decrease in the corresponding activated energy gap Δ, calculated using the equation $\rho(T) = \rho_0 e^{\Delta/2k_BT}$, where ρ_0 is a constant, both saturate at pressures that correlate with the transition pressure P_t, into the high-T_c superconducting phase. In the specific case of $NdO_{0.5}F_{0.5}BiS_2$, a semiconductor to metal phase transition occurs at P_t. These changes in the normal-state electrical resistivity indicate that there may

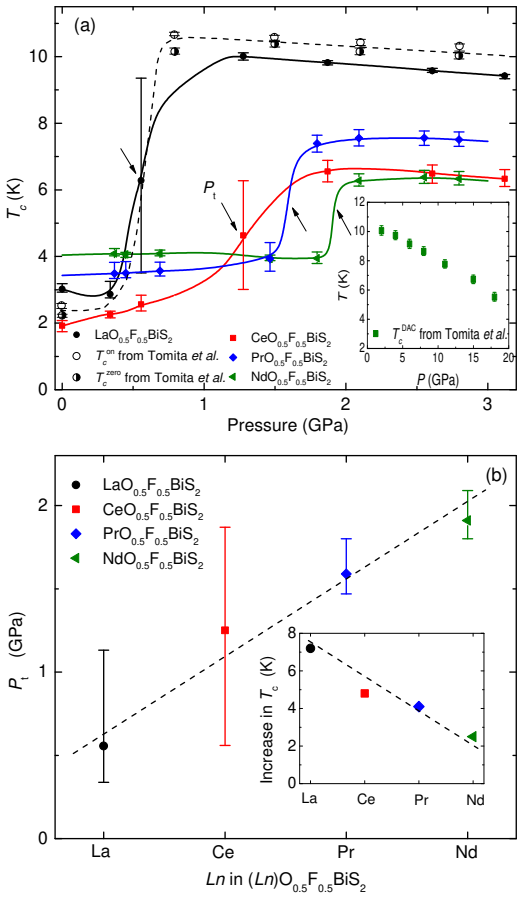

Figure 21: (Color online) (a) T_c vs. pressure for the compounds $LnO_{0.5}F_{0.5}BiS_2$ (Ln = La, Ce, Pr, Nd) [17, 18, 19]. The black arrows identify the phase transition pressure P_t which is defined in the text. The inset displays the $P-T$ phase diagram for $LaO_{0.5}F_{0.5}BiS_2$ up to $P \approx 18$ GPa [19]. (b) Phase transition pressure P_t plotted as a function of Ln. The inset displays the increase in T_c at P_t as a function of Ln. Dashed lines are guides to the eye (after Wolowiec *et al.* [17, 18] and Tomita *et al.* [19]).

be significant increases in the charge-carrier density during the rapid enhancement in T_c that occurs between the two superconducting phases [18].

The transition pressures P_t, indicated by the black arrows in the temperature-pressure phase diagrams of Fig. 21(a), were defined as the pressure corresponding to the value of T_c at the midpoint between the values of T_c in the low and high T_c phases immediately preceding and following the transition. P_t is plotted as a function of lanthanide element (Ln = La, Ce, Pr, Nd) in $LnO_{0.5}F_{0.5}BiS_2$ in Fig. 21(b). There is a clear linear relationship between the increase in atomic number of the Ln and an increase in P_t. The magnitude of the "jump" in T_c also scales with the atomic number of the Ln element in $LnO_{0.5}F_{0.5}BiS_2$ as is clearly shown in the inset of Fig. 21(b). The pressure-induced increase in T_c decreases in magnitude as the atomic number of the lanthanide element increases. The lengths of the vertical bars in Fig. 21(b) represent the respective pressure windows over which the transitions from the low T_c phase to the high T_c phase occurred in each of the four compounds. Further electrical resistivity and magnetization measurements up to an applied pressure $P \approx 18$ GPa were performed by Tomita *et al.*[19] and McElroy *et al.* [95]. The P-T_c phase diagram, determined by electrical resistivity measurements up to $P \approx 3$ GPa, is presented in Fig. 21(a), and $T_c(P)$ up to $P \approx 18$ Gpa is shown in the inset where $T_{c,zero}$ and $T_{c,on}$ are defined as the zero-resistance and onset temperatures, respectively. In the pressure range 0 - 0.7 GPa, $T_c(P)$ is roughly constant (~2.6 K) and T_c markedly increases to T_{max} = 10.7 K at P_t, which is very close to the temperature determined by Wolowiec *et al.* [18]. This maximum T_c is comparable to that for HP annealed samples of $LaO_{0.5}F_{0.5}BiS_2$ at ambient pressure. Above P_t, T_c decreases linearly which is consistent with the phase diagram determined by Wolowiec *et al.* [18]. T_c is initially suppressed at a rate of $dT_c/dP \simeq$ -0.28 K/GPa; this result is comparable to the initial suppression rate of $dT_c/dP \simeq$ -0.4 K/GPa, obtained from measurements on a $LaO_{0.5}F_{0.5}BiS_2$ sample synthesized using the HP annealing technique.

The scaling of both the phase transition pressure P_t and the size of the "jump" in T_c with the atomic number of the lanthanide element suggests that the pressure-induced phase transition between the two superconducting phases may be a structural transition. To investigate that claim, X-ray diffraction measurements on $LaO_{1-x}F_xBiS_2$ (x = 0, 0.5) were performed under applied pressure. As displayed in Fig. 22(a), the X-ray diffraction pattern of $LaO_{0.5}F_{0.5}BiS_2$ (AP samples) obtained at room temperature is consistent with the same tetragonal structure ($P4/nmm$) as the ambient pressure pattern with lattice parameters a = 4.0877 and c = 13.4703 Å [19, 96]. A splitting near $2\theta \approx 23.5°$ appears in the diffraction pattern at 0.85 GPa, which develops with increasing pressure. Above 1.5 GPa, $LaO_{0.5}F_{0.5}BiS_2$ undergoes a complete structural phase transition from tetragonal ($P4/nmm$) to monoclinic ($P2_1/m$). The pressure-induced structural phase transition from tetragonal to monoclinic ($P2_1/m$) occurs at ~0.8 GPa, which corresponds well to P_t. This structural phase transition is also observed at ~2 GPa in $LaOBiS_2$. 2×2×1 unit cells for the tetragonal $P4/nmm$ structure at 0.4 GPa and monoclinic $P2_1/m$ structure at 3.8 GPa

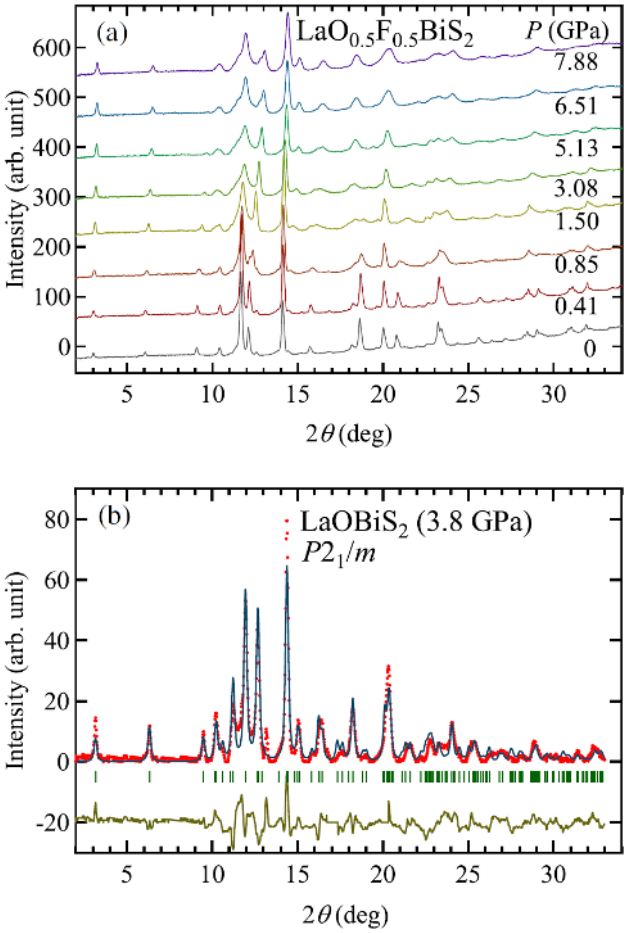

Figure 22: (Color online) (a) X-ray diffraction patterns for $LaO_{0.5}F_{0.5}BiS_2$, obtained using Mo Kα X-rays at room temperature under applied pressures up to 8 GPa. (b) X-ray diffraction pattern and Reitveld refinement fitting for $LaOBiS_2$, using Kα X-rays at room temperature under an applied pressure of 3.8 GPa. The background is subtracted from the pattern in this figure (after Tomita *et al.* [19]).

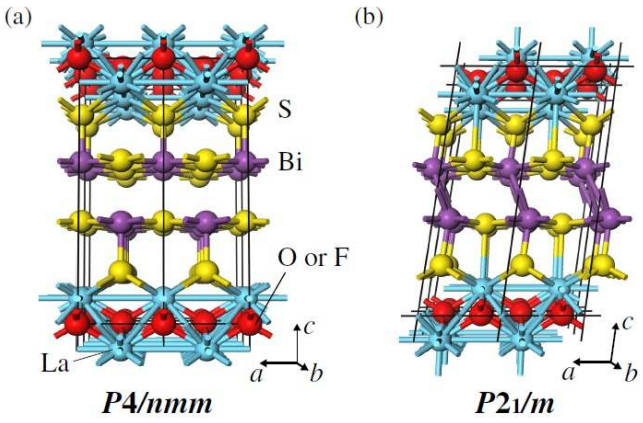

Figure 23: (Color online) 2×2×1 unit cells for the (a) tetragonal $P4/nmm$ crystal structure at 0.4 GPa and (b) monoclinic $P2_1/m$ crystal structure at 3.8 GPa, viewed along the b axis (after Tomita *et al.* [19]).

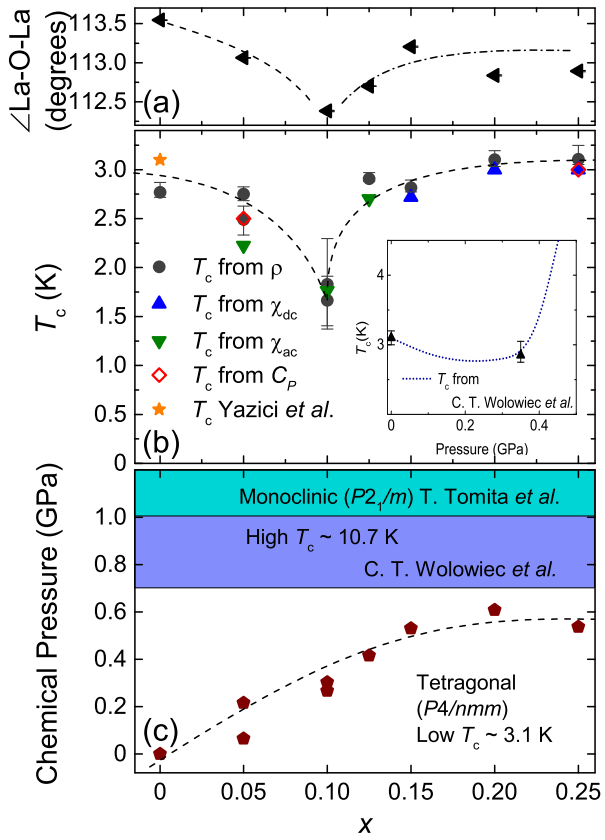

Figure 24: (Color online) (a) La/Y-O/F-La/Y bond angle ∠La-O-La vs. nominal yttrium concentration x. (b) Superconducting transition temperature T_c vs. nominal yttrium concentration x for the $La_{1-x}Y_xO_{0.5}F_{0.5}BiS_2$ system. The orange star is the maximum T_c obtained from electrical resistivity measurements of $LaO_{0.5}F_{0.5}BiS_2$ reported in Ref. [8]. The inset shows the behavior of T_c under applied pressure [17]. (c) Chemical pressure vs. nominal yttrium concentration. Two regions with low T_c and high T_c (purple and blue regions) are separated by the reported critical pressure value $P_c \sim 0.7$ GPa [15, 17, 19]. The tetragonal (unfilled and purple regions) and monoclinic (blue region) phases are distinguished by the critical pressure $P_t \sim 1$ GPa for the structural phase transition [19] (after Jeon *et al.* [78]).

are shown in Figs. 23(a) and (b).

As it has been reported, the compounds $LnO_{0.5}F_{0.5}BiS_2$ (*Ln* = La, Ce, Pr, Nd) show remarkable enhancements of T_c when subjected to applied pressure [17, 18]. To investigate the relationships between pressure, lattice parameters, and superconductivity, the chemical substitution of Y for La has been recently reported [78]. Jeon *et al.* established a relationship between T_c and crystal structure details in $La_{1-x}Y_xO_{0.5}F_{0.5}BiS_2$. As shown in Figs. 24(a) and (b), $T_c(x)$ is related to the lattice constant c and/or the La-O-La bond angle. The effect of chemical pressure on the variation of T_c was also discussed, since the unit cell volume V decreases with increasing Y concentration. A plot of chemical pressure vs. the nominal Y concentration x in Fig. 24(c) shows that chemical pressure increases with Y concentrations $0 \leq x \leq 0.20$ and saturates at a value of ~0.6 GPa at the solubility limit. It is clear that the chemical pressure is insufficient to induce the high-T_c or the monoclinic phase. If the chemical pressure could be further increased, the high-T_c and monoclinic phases would likely be induced for $x \geq 0.20$. Under applied pressure, the lattice parameters a and c of $LaO_{0.5}F_{0.5}BiS_2$ decrease continuously until a structural phase transition is induced near 1 GPa [19]. However, chemical pressure is insufficient to induce the structural phase transition. The initial suppression and subsequent enhancement of T_c with x appears to be correlated with the variation of the La-O/F-La bond angle with x as shown in Figs. 24 (a) and (b); in agreement with other studies [37, 46], this observation strongly suggests that T_c is tuned by crystal structure details in the BiS_2-based superconducting systems.

15. Concluding remarks

In this article, we have reviewed the intensive research that has been carried out on the BiS_2-based superconductors since the discovery of this class of superconducting materials in 2012. These compounds have layered crystal structures that consist of alternate stacking of superconducting BiS_2 and blocking layers. This stacking structure is analogous to those of high-T_c cuprates and Fe-based superconductors. Typically, superconductivity in BiS_2-based compounds arises when charge carriers are introduced into the parent compound, and the superconducting transition temperature T_c reaches a maximum value at the nominal concentration of 0.5 electrons per $LnOBiS_2$ formula unit [6, 10]. First principles calculations indicate that the parent compound is a semiconductor with an energy gap of ~0.8 eV, and that superconductivity is induced by electron doping and is associated mainly with the $6p_x/p_y$ orbitals in the BiS_2 layers [21, 58]. At $x = 0.5$, a good nesting condition has been found between the large parallel Fermi-surface segments with wave vector $q = (\pi, \pi, 0)$. It was therefore suggested that the BiS_2-based superconductors are conventional phonon-mediated superconductors, close to a CDW instability [58, 40]. However, this picture was not supported by a subsequent neutron scattering experiment [39]. The electron-phonon coupling could be much weaker than theoretically expected. It was also proposed that the strong Fermi surface nesting could enhance the spin fluctuations, and that electronic correlations may play a major role in superconducting pairing [20, 59, 41, 65]. At present, there is no consensus on the origin of superconductivity in these compounds.

It is important to distinguish between the different possible mechanisms underlying superconductivity scenarios in these materials by performing a wide range of experimental investigations. Most of the early studies have been conducted on polycrystalline samples. Recently, millimeter-sized single crystals were successfully grown from an alkali-metal-chloride flux in vacuum [28, 26], and two ARPES studies on the electronic structures of $NdO_{1-x}F_xBiS_2$ were reported [74, 80]. Ye *et al.* found that the electronic correlations are very weak and that the charge carrier doping is much smaller than that expected from the nominal fluorine concentration; they attributed this to a bismuth deficiency in the single crystals [74]. Another ARPES study reported by Zeng *et al.* also reveals rather small electron pockets around the X point, corresponding to an electron doping level of roughly 7% per Bi site [80]. Optical spectroscopy

measurements [22] reveal a simple metallic response with a plasma frequency of 2.1 eV. Assuming a doping level of 7% of itinerant electrons per Bi site, as determined by ARPES experiments on the same batch of crystals, band-structure calculations yield almost the same plasma frequency. Furthermore, the interband transitions at higher energies, observed in optical measurements, are also reproduced by the band-structure calculations. These results reveal an absence of correlation effects in the compound. This study also indicates that superconducting samples with these electron concentrations are far from any CDW instability, which was widely discussed for samples with $x = 0.5$. Consequently, many of the early theoretical studies, based on higher electron concentrations (close to $x = 0.5$), were not applicable to the lower electron concentration levels encountered in the actual experiments. Additional experiments on single crystals will be very useful in establishing the physical properties of BiS_2-based superconductors with greater confidence.

Motivated by the discovery of superconductivity in $Bi_4O_4S_3$, new materials which were not previously investigated have been synthesized and studied. Many of the materials discussed in this review were discovered through this process. There are many reports concerning chemical substitution effects within the blocking layers on T_c in the systems $Sr_{0.5}R_{0.5}FBiS_2$ (R = Ce, Nd, Pr, and Sm) [97], $Ce_{1-x}Nd_xO_{1-y}F_yBiS_2$, $Nd_{1-z}Sm_zO_{1-y}F_yBiS_2$ [98, 99], and $La_{1-x}Sm_xO_{0.5}F_{0.5}BiS_2$ [79], and also a few studies investigating the chemical substitution effects within the superconducting BiS_2 layer, *i.e.*, $NdO_{0.5}F_{0.5}Bi(S_{1-x}Se_x)_2$ and $NdO_{0.5}F_{0.5}Bi_{1-y}Sb_yS_2$ [100]. These latter studies are important because changes in the lattice constants are generated without any change in the carrier concentration. Less well known are studies of materials that did not exhibit superconductivity but are nevertheless important. For example, the compounds $LaO_{0.5}F_{0.5}BiTe_2$ and $LaO_{0.5}F_{0.5}SbS_2$ do not exhibit superconductivity down to $T = 1.7$ K [12].

As has been repeatedly proven in the past, new materials research is one of the main avenues for quantum leaps in our understanding of complex and unresolved condensed matter and materials physics issues. As a community, we should continue to pursue the dream of room-temperature superconductivity through a continuing program of new materials research. As a collateral benefit, exciting discoveries in other contexts are bound to occur along the way.

Acknowledgements

Preparation of this manuscript was performed with financial support from the U.S. Department of Energy, Office of Basic Energy Sciences, Division of Materials Sciences and Engineering under Award Grant No. DE-FG02-04-ER46105, the National Nuclear Security Administration under the Stewardship Science Academic Alliance program through the U.S. Department of Energy Grant No. DENA0001841, and the National Science Foundation under Grant No. DMR-1206553.

References

[1] Y. Mizuguchi, H. Fujihisa, Y. Gotoh, K. Suzuki, H. Usui, K. Kuroki, S. Demura, Y. Takano, H. Izawa, O. Miura, Novel BiS_2-based layered superconductor $Bi_4O_4S_3$, Phys. Rev. B 86 (2012) 220510(R).

[2] E. Dagotto, Correlated electrons in high-temperature superconductors, Rev. Mod. Phys. 66 (1994) 763.

[3] P. A. Lee, N. Nagaosa, X.-G. Wen, Doping a Mott insulator: Physics of high-temperature superconductivity, Rev. Mod. Phys. 78 (2006) 17.

[4] J. Paglione, R. L. Greene, High-temperature superconductivity in iron-based materials, Nat. Phys. 6 (2010) 645.

[5] D. C. Johnston, The puzzle of high temperature superconductivity in layered iron pnictides and chalcogenides, Adv. Phys. 59 (2010) 803.

[6] Y. Mizuguchi, S. Demura, K. Deguchi, Y. Takano, H. Fujihisa, Y. Gotoh, H. Izawa, O. Miura, Superconductivity in novel BiS_2-based layered superconductor $LaO_{1-x}F_xBiS_2$, J. Phys. Soc. Jpn. 81 (2012) 114725.

[7] Y. Mizuguchi, T. Hiroi, J. Kajitani, H. Takatsu, H. Kadowaki, O. Miura, Stabilization of high-T_c phase of BiS_2-based superconductor $LaO_{0.5}F_{0.5}BiS_2$ using high-pressure synthesis, J. Phys. Soc. Jpn. 83 (2014) 053704.

[8] D. Yazici, K. Huang, B. D. White, A. H. Chang, A. J. Friedman, M. B. Maple, Superconductivity of F-substituted LnOBiS$_2$ (Ln = La, Ce, Pr, Nd, Yb) compounds, Phil. Mag. 93 (2013) 673.

[9] G. R. Stewart, Superconductivity in iron compounds, Rev. Mod. Phys. 83 (2011) 1589.

[10] S. Demura, Y. Mizuguchi, K. Deguchi, H. Okazaki, H. Hara, T. Watanabe, S. James Denholme, M. Fujioka, T. Ozaki, H. Fujihisa, Y. Gotoh, O. Miura, T. Yamaguchi, H. Takeya, Y. Takano, New member of BiS_2-based superconductor $NdO_{1-x}F_xBiS_2$, J. Phys. Soc. Jpn. 82 (2013) 033708.

[11] D. Yazici, K. Huang, B. D. White, I. Jeon, V. W. Burnett, A. J. Friedman, I. K. Lum, M. Nallaiyan, S. Spagna, M. B. Maple, Superconductivity induced by electron doping in $La_{1-x}M_x$OBiS$_2$ (M = Ti, Zr, Hf, Th), Phys. Rev. B 87 (2013) 174512.

[12] A. Krzton-Maziopa, Z. Guguchia, E. Pomjakushina, V. Pomjakushin, R. Khasanov, H. Luetkens, P. K. Biswas, A. Amato, H. Keller, K. Conder, Superconductivity in a new layered bismuth oxyselenide: $LaO_{0.5}F_{0.5}BiSe_2$, J. Phys.: Condens. Matter 26 (2014) 215702.

[13] M. Tanaka, M. Nagao, Y. Matsushita, M. Fujioka, S. J. Denholme, T. Yamaguchi, H. Takeya, Y. Takano, First single crystal growth and structural analysis of superconducting layered bismuth oxyselenide; La(O,F)BiSe$_2$, J. Solid State Chem. 219 (2014) 168.

[14] M. Nagao, M. Tanaka, S. Watauchi, I. Tanaka, Y. Takano, Superconducting anisotropies of F-substituted LaOBiSe$_2$ single crystals, J. Phys. Soc. Jpn. 83 (2014) 114709.

[15] H. Kotegawa, Y. Tomita, H. Tou, H. Izawa, Y. Mizuguchi, O. Miura, S. Demura, K. Deguchi, Y. Takano, Pressure Study of BiS_2-Based Superconductors $Bi_4O_4S_3$ and La(O,F)BiS$_2$, J. Phys. Soc. Jpn. 81 (2012) 103702.

[16] G. Selvan Kalai, M. Kanagaraj, S. Esakki Muthu, R. Jha, V. P. S. Awana, S. Arumugam, Hydrostatic pressure effect on T_c of new BiS_2-based $Bi_4O_4S_3$ and $NdO_{0.5}F_{0.5}BiS_2$ layered superconductors, Phys. Stat. Solidi Rapid Res. Lett. 7 (2013) 510.

[17] C. T. Wolowiec, D. Yazici, B. D. White, K. Huang, M. B. Maple, Pressure-induced enhancement of superconductivity and suppression of semiconducting behavior in $Ln O_{0.5}F_{0.5}BiS_2$ (Ln = La, Ce) compounds, Phys. Rev. B 88 (2013) 064503.

[18] C. T. Wolowiec, B. D. White, I. Jeon, D. Yazici, K. Huang, M. B. Maple, Enhancement of superconductivity near the pressure-induced semiconductor-metal transition in the BiS_2-based superconductors $Ln O_{0.5}F_{0.5}BiS_2$ (Ln = La, Ce, Pr, Nd), J. Phys.: Condens. Matter 25 (2013) 422201.

[19] T. Tomita, M. Ebata, H. Soeda, H. Takahashi, H. Fujihisa, Y. Gotoh, Y. Mizuguchi, H. Izawa, O. Miura, S. Demura, K. Deguchi, Y. Takano, Pressure-induced enhancement of superconductivity and structural transition in BiS_2-layered $LaO_{1-x}F_xBiS_2$, J. Phys. Soc. Jpn. 83 (2014) 063704.

[20] T. Yildirim, Ferroelectric soft phonons, charge density wave instability, and strong electron-phonon coupling in BiS_2 layered superconductors: A first-principles study, Phys. Rev. B 87 (2013) 020506.

[21] H. Usui, K. Suzuki, K. Kuroki, Minimal electronic models for superconducting BiS_2 layers, Phys. Rev. B 86 (2012) 220501.

[22] X. B. Wang, S. M. Nie, H. P. Wang, P. Zheng, P. Wang, T. Dong, H. M. Weng, N. L. Wang, Optical spectroscopy study of Nd(O,F)BiS_2 single crystals, Phys. Rev. B 90 (2014) 054507.

[23] K. Kuroki, S. Onari, R. Arita, H. Usui, Y. Tanaka, H. Kontani, H. Aoki, Unconventional pairing originating from the disconnected Fermi surfaces of superconducting $LaFeAsO_{1-x}F_x$, Phys. Rev. Lett. 101 (2008) 087004.

[24] I. C. Sathish, H. L. Feng, Y. Shi, K. Yamaura, Superconductivity in Bismuth Oxysulfide $Bi_4O_4S_3$, J. Phys. Soc. Jpn. 82 (2013) 074703.

[25] W. A. Phelan, D. C. Wallace, K. E. Arpino, J. R. Neilson, K. J. Livi, C. R. Seabourne, A. J. Scott, T. M. McQueen, Stacking Variants and Superconductivity in the Bi-O-S System, J. Am. Chem. Soc. 135 (2013) 5372.

[26] J. Liu, D. Fang, Z. Wang, J. Xing, Z. Du, S. Li, X. Zhu, H. Yang, H.-H. Wen, Giant superconducting fluctuation and anomalous semiconducting normal state in $NdO_{1-x}F_xBiS_2$ single crystals, Europhys. Lett. 106 (2014) 67002.

[27] M. Nagao, A. Miura, S. Demura, K. Deguchi, S. Watauchi, T. Takei, Y. Takano, N. Kumada, I. Tanaka, Growth and superconducting properties of F-substituted $ROBiS_2$ (R = La, Ce, Nd) single crystals, Solid State Comm. 178 (2014) 33.

[28] M. Nagao, S. Demura, K. Deguchi, A. Miura, S. Watauchi, T. Takei, Y. Takano, N. Kumada, I. Tanaka, Structural analysis and superconducting properties of F-Substituted $NdOBiS_2$ single crystals, J. Phys. Soc. Jpn. 82 (2013) 113701.

[29] Cornell university library, URL: http://arxiv.org/archive/cond-mat.

[30] P. K. Biswas, A. Amato, C. Baines, R. Khasanov, H. Luetkens, H. Lei, C. Petrovic, E. Morenzoni, Low superfluid density and possible multigap superconductivity in the BiS_2-based layered superconductor $Bi_4O_4S_3$, Phys. Rev. B 88 (2013) 224515.

[31] S. Li, H. Yang, D. Fang, Z. Wang, J. Tao, X. Ding, H. Wen, Strong coupling superconductivity and prominent superconducting fluctuations in the new superconductor $Bi_4O_4S_3$, Sci. China Phys. Mech. Astron. 56 (2013) 2019.

[32] Shruti, P. Srivastava, S. Patnaik, Evidence for fully gapped strong coupling s-wave superconductivity in $Bi_4O_4S_3$, J. of Phys.: Condens. Matter 25 (2013) 312202.

[33] S. K. Singh, A. Kumar, B. Gahtori, S. K., G. Sharma, S. Patnaik, V. P. S. Awana, Bulk Superconductivity in Bismuth Oxysulfide $Bi_4O_4S_3$, J. Am. Chem. Soc. 134 (2012) 16504.

[34] S. Tan, L. Li, Y. Liu, P. Tong, B. Zhao, W. Lu, Y. Sun, Superconducting and thermoelectric properties of new layered superconductor $Bi_4O_4S_3$, Physica C 483 (2012) 94.

[35] H. Takatsu, Y. Mizuguchi, H. Izawa, O. Miura, H. Kadowaki, Bulk superconductivity in $Bi_4O_4S_3$ revealed by specific heat measurement, J. Phys. Soc. Jpn. 81 (2012) 125002.

[36] K. Deguchi, Y. Mizuguchi, S. Demura, H. Hara, T. Watanabe, S. J. Denholme, M. Fujioka, H. Okazaki, T. Ozaki, H. Takeya, T. Yamaguchi, O. Miura, Y. Takano, Evolution of superconductivity in $LaO_{1-x}F_xBiS_2$ prepared by high-pressure technique, Europhys. Lett. 101 (2013) 17004.

[37] J. Kajitani, K. Deguchi, A. Omachi, T. Hiroi, Y. Takano, H. Takatsu, H. Kadowaki, O. Miura, Y. Mizuguchi, Correlation between crystal structure and superconductivity in $LaO_{0.5}F_{0.5}BiS_2$, Solid State Comm. 181 (2014) 1.

[38] G. Lamura, T. Shiroka, P. Bonfà, S. Sanna, R. De Renzi, C. Baines, H. Luetkens, J. Kajitani, Y. Mizuguchi, O. Miura, K. Deguchi, S. Demura, Y. Takano, M. Putti, s-wave pairing in the optimally doped $LaO_{0.5}F_{0.5}BiS_2$ superconductor, Phys. Rev. B 88 (2013) 180509.

[39] J. Lee, M. B. Stone, A. Huq, T. Yildirim, G. Ehlers, Y. Mizuguchi, O. Miura, Y. Takano, K. Deguchi, S. Demura, S.-H. Lee, Crystal structure, lattice vibrations, and superconductivity of $LaO_{1-x}F_xBiS_2$, Phys. Rev. B 87 (2013) 205134.

[40] B. Li, Z. W. Xing, G. Q. Huang, Phonon spectra and superconductivity of the BiS_2-based compounds $LaO_{1-x}F_xBiS_2$, Europhys. Lett. 101 (2013) 47002.

[41] Y. Liang, X. Wu, W.-F. Tsai, J. Hu, Pairing symmetry in layered BiS_2 compounds driven by electron-electron correlation, Frontiers Phys. 9 (2014) 194.

[42] V. Awana, A. Kumar, R. Jha, S. Shiva Kumar, A. Pal, K. Shruti, J. Saha, S. Patnaik, Appearance of superconductivity in layered $LaO_{0.5}F_{0.5}BiS_2$, Solid State Comm. 157 (2013) 21.

[43] J. Xing, S. Li, X. Ding, H. Yang, H. Wen, Superconductivity appears in the vicinity of semiconducting-like behavior in $CeO_{1-x}F_xBiS_2$, Phys. Rev. B 86 (2012) 214518.

[44] T. Sugimoto, B. Joseph, E. Paris, A. Iadecola, T. Mizokawa, S. Demura, Y. Mizuguchi, Y. Takano, N. L. Saini, Role of the Ce valence in the coexistence of superconductivity and ferromagnetism of $CeO_{1-x}F_xBiS_2$ revealed by Ce L_3-edge x-ray absorption spectroscopy, Phys. Rev. B 89 (2014) 201117.

[45] R. Jha, V. Awana, Superconductivity in Layered $CeO_{0.5}F_{0.5}BiS_2$, J. Superconductivity Novel Mag. 27 (2014) 1.

[46] J. Kajitani, K. Deguchi, T. Hiroi, A. Omachi, S. Demura, Y. Takano, O. Miura, Y. Mizuguchi, Enhancement of T_c by uniaxial lattice contraction in BiS_2-based superconductor $PrO_{0.5}F_{0.5}BiS_2$, J. Phys. Soc. Jpn. 83 (2014) 065002.

[47] R. Jha, H. Kishan, V. P. S. Awana, Superconducting and magnetotransport properties of BiS_2 based superconductor $PrO_{1-x}F_xBiS_2$ (x = 0 to 0.9), J. Appl. Phys. 115 (2014) 013902.

[48] T. Machida, Y. Fujisawa, M. Nagao, S. Demura, K. Deguchi, Y. Mizuguchi, Y. Takano, H. Sakata, Checkerboard stripe electronic state on cleaved surface of $NdO_{0.7}F_{0.3}BiS_2$ probed by scanning tunneling microscope (2014). arXiv:1403.6110.

[49] R. Jha, A. Kumar, S. Kumar Singh, V. P. S. Awana, Superconductivity at 5 K in $NdO_{0.5}F_{0.5}BiS_2$, J. Appl. Phys. 113 (2013) 056102.

[50] X. Lin, X. Ni, B. Chen, X. Xu, X. Yang, J. Dai, Y. Li, X. Yang, Y. Luo, Q. Tao, G. Cao, Z. Xu, Superconductivity induced by La doping in $Sr_{1-x}La_xFBiS_2$, Phys. Rev. B 87 (2013) 020504.

[51] R. Jha, B. Tiwari, V. P. S. Awana, Impact of Hydrostatic Pressure on Superconductivity of $Sr_{0.5}La_{0.5}FBiS_2$, J. Phys. Soc. Jpn. 83 (2014) 063707.

[52] Zhai, Hui-Fei and Tang, Zhang-Tu and Jiang, Hao and Xu, Kai and Zhang, Ke and Zhang, Pan and Bao, Jin-Ke and Sun, Yun-Lei and Jiao, Wen-He and Nowik, I. and Felner, I. and Li, Yu-Ke and Xu, Xiao-Feng and Tao, Qian and Feng, Chun-Mu and Xu, Zhu-An and Cao, Guang-Han, Possible charge-density wave, superconductivity, and f-electron valence instability in $EuBiS_2F$, Phys. Rev. B 90 (2014) 064518.

[53] C. C. Tsuei, J. R. Kirtley, Pairing symmetry in cuprate superconductors, Rev. Mod. Phys. 72 (2000) 969.

[54] I. I. Mazin, Superconductivity gets an iron boost, Nature 464 (2010) 183.

[55] P. Srivastava, Shruti, S. Patnaik, Structural, electromagnetic and thermoelectric properties of $Bi_4O_4S_3$ superconductor, Superconduct. Science Tech. 27 (2014) 055001.

[56] J. Kajitani, T. Hiroi, A. Omachi, O. Miura, Y. Mizuguchi, Increase in T_c and change of crystal structure by high-pressure annealing in BiS_2-based superconductor $CeO_{0.3}F_{0.7}BiS_2$ (2014). arXiv:1404.6361.

[57] A. Miura, M. Nagao, T. Takei, S. Watauchi, I. Tanaka, N. Kumada, Crystal structures of $LaO_{1-x}F_xBiS_2$ ($x \sim 0.23, 0.46$): Effect of F doping on distortion of Bi-S plane, J. Solid State Chem. 212 (2014) 213.

[58] X. Wan, H.-C. Ding, S. Y. Savrasov, C.-G. Duan, Electron-phonon superconductivity near charge-density-wave instability in $LaO_{0.5}F_{0.5}BiS_2$: Density-functional calculations, Phys. Rev. B 87 (2013) 115124.

[59] T. Zhou, Z. Wang, Probing the superconducting pairing symmetry from spin excitations in BiS_2 based superconductors, J. Superconductivity Novel Mag. 26 (2013) 2735.

[60] S. L. Liu, Impurity effect as a probe of the pairing symmetry in BiS_2-based superconductors, J. Superconductivity Novel Mag. 26 (2013) 3411.

[61] I. R. Shein, A. L. Ivanovskii, Electronic band structure and Fermi surface for new layered superconductor $LaO_{0.5}F_{0.5}BiS_2$ in comparison with parent phase $LaOBiS_2$ from first principles, JETP Letters 96 (2013) 769.

[62] K. Suzuki, H. Usui, K. Kuroki, Minimum Model and its Theoretical Analysis for Superconducting Materials with BiS_2 Layers, Phys. Procedia 45 (2013) 21, proceedings of the 25th International Symposium on Superconductivity (ISS2012).

[63] G. B. Martins, A. Moreo, E. Dagotto, RPA analysis of a two-orbital model for the BiS_2-based superconductors, Phys. Rev. B 87 (2013) 081102.

[64] Y. Gao, Pairing symmetry in BiS_2-based superconductors (2013). arXiv:1304.2102.

[65] Y. Yang, W.-S. Wang, Y.-Y. Xiang, Z.-Z. Li, Q.-H. Wang, Triplet pairing and possible weak topological superconductivity in BiS_2-based superconductors, Phys. Rev. B 88 (2013) 094519.

[66] C. Morice, E. Artacho, S. E. Dutton, D. Molnar, H.-J. Kim, S. S. Saxena,

Electronic and magnetic properties of superconducting $LnO_{1-x}F_xBiS_2$ (Ln = La, Ce, Pr, and Nd) from first principles (2013). arXiv:1312.2615.
[67] X. Wu, J. Yuan, Y. Liang, H. Fan, J. Hu, g-wave Pairing in BiS_2-based Superconductors (2014). arXiv:1403.5949.
[68] H. Yao, F. Yang, Topological odd-parity superconductivity at Type-II 2D Van Hove singularities (2013). arXiv:1312.0077.
[69] Y. Feng, H.-C. Ding, Y. Du, X. Wan, B. Wang, S. Y. Savrasov, C.-G. Duan, Electron-phonon superconductivity in $LaO_{0.5}F_{0.5}BiSe_2$, J. Appl. Phys. 115 (2014) 233901.
[70] A. C. Larson, R. B. Von Dreele, General Structure Analysis System (GSAS) (2000).
[71] J. Xing, S. Li, X. Ding, H. Yang, H.-H. Wen, Superconductivity appears in the vicinity of semiconducting-like behavior in $CeO_{1-x}F_xBiS_2$, Phys. Rev. B 86 (2012) 214518.
[72] L. Li, Y. Li, Y. Jin, H. Huang, B. Chen, X. Xu, J. Dai, L. Zhang, X. Yang, H. Zhai, G. Cao, Z. Xu, Coexistence of superconductivity and ferromagnetism in $Sr_{0.5}Ce_{0.5}FBiS_2$ (2014). arXiv:1407.3711.
[73] M. A. McGuire, A. D. Christianson, A. S. Sefat, B. C. Sales, M. D. Lumsden, R. Jin, E. A. Payzant, D. Mandrus, Y. Luan, V. Keppens, V. Varadarajan, J. W. Brill, R. P. Hermann, M. T. Sougrati, F. Grandjean, G. J. Long, Phase transitions in LaFeAsO: Structural, magnetic, elastic, and transport properties, heat capacity and Mössbauer spectra, Phys. Rev. B 78 (2008) 094517.
[74] Z. R. Ye, H. F. Yang, D. W. Shen, J. Jiang, X. H. Niu, D. L. Feng, Y. P. Du, X. G. Wan, J. Z. Liu, X. Y. Zhu, H. H. Wen, M. H. Jiang, Electronic structure of single-crystalline $NdO_{0.5}F_{0.5}BiS_2$ studied by angle-resolved photoemission spectroscopy, Phys. Rev. B 90 (2014) 045116.
[75] J. M. Luttinger, J. C. Ward, Ground-State Energy of a Many-Fermion System. II, Phys. Rev. 118 (1960) 1417.
[76] J. M. Luttinger, Fermi Surface and Some Simple Equilibrium Properties of a System of Interacting Fermions, Phys. Rev. 119 (1960) 1153.
[77] S. Nagira, J. Sonoyama, T. Wakita, M. Sunagawa, Y. Izumi, T. Muro, H. Kumigashira, M. Oshima, K. Deguchi, H. Okazaki, Y. Takano, O. Miura, Y. Mizuguchi, K. Suzuki, H. Usui, K. Kuroki, K. Okada, Y. Muraoka, T. Yokoya, Soft x-ray photoemission study of new BiS_2-layered superconductor $LaO_{1-x}F_xBiS_2$, J. Phys. Soc. Jpn. 83 (2014) 033703.
[78] I. Jeon, D. Yazici, B. D. White, A. J. Friedman, M. B. Maple, Effect of yttrium substitution on the superconducting properties of $La_{1-x}Y_xO_{0.5}F_{0.5}BiS_2$, Phys. Rev. B 90 (2014) 054510.
[79] Y. Fang, D. Yazici, B. D. White, M. B. Maple, Enhancement of superconductivity in $La_{1-x}Sm_xO_{0.5}F_{0.5}BiS_2$ (2014). arXiv:1410.0061.
[80] L. K. Zeng, X. B. Wang, J. Ma, P. Richard, S. M. Nie, H. M. Weng, N. L. Wang, Z. Wang, T. Qian, H. Ding, Observation of anomalous temperature dependence of spectrum on small Fermi surfaces in a BiS_2-based superconductor, Phys. Rev. B 90 (2014) 054512.
[81] S. Demura, K. Deguchi, Y. Mizuguchi, K. Sato, R. Honjyo, A. Yamashita, T. Yamaki, H. Hara, T. Watanabe, S. J. Denholme, M. Fujioka, H. Okazaki, T. Ozaki, O. Miura, T. Yamaguchi, H. Takeya, Y. Takano, Coexistence of bulk superconductivity and ferromagnetism in $CeO_{1-x}F_xBiS_2$ (2013). arXiv:1311.4267.
[82] H. Matsuyama, I. Harada, A. Kotani, Roles of $4f-5d$ exchange interactions in magnetic circular x-ray dichroism at the Rare-Earth $L_{2,3}$ Edges, J. Phys. Soc. Jpn. 66 (1997) 337.
[83] C. Krellner, T. Förster, H. Jeevan, C. Geibel, J. Sichelschmidt, Relevance of Ferromagnetic Correlations for the Electron Spin Resonance in Kondo Lattice Systems, Phys. Rev. Lett. 100 (2008) 066401.
[84] D. Gignoux, J. C. Gomez-Sal, Competition between the Kondo effect and exchange interactions in the $CeNi_xPt_{1-x}$ compounds, Phys. Rev. B 30 (1984) 3967.
[85] B. H. Grier, J. M. Lawrence, V. Murgai, R. D. Parks, Magnetic ordering in CeM_2Si_2 (M = Ag, Au, Pd, Rh) compounds as studied by neutron diffraction, Phys. Rev. B 29 (1984) 2664.
[86] S. K. Malik, D. T. Adroja, CePdSb: A possible ferromagnetic Kondo-lattice system, Phys. Rev. B 43 (1991) 6295.
[87] H. Sakai, D. Kotajima, K. Saito, H. Wadati, Y. Wakisaka, M. Mizumaki, K. Nitta, Y. Tokura, S. Ishiwata, Insulator-to-Superconductor Transition upon Electron Doping in a BiS_2-Based Superconductor $Sr_{1-x}La_xFBiS_2$, J. Phys. Soc. Jpn. 83 (2014) 014709.
[88] Y. Mizuguchi, A. Miyake, K. Akiba, M. Tokunaga, J. Kajitani, O. Miura, Anisotropic upper critical field of the BiS_2-based superconductor $LaO_{0.5}F_{0.5}BiS_2$, Phys. Rev. B 89 (2014) 174515.
[89] R. Jha, V. P. S. Awana, Superconducting properties of BiS_2 based superconductor $NdO_{1-x}F_xBiS_2$ (x = 0 to 0.9), Mater. Res. Express 1 (2014) 016002.
[90] N. R. Werthamer, E. Helfand, P. C. Hohenberg, Temperature and Purity Dependence of the Superconducting Critical Field, H_{c2}. III. Electron Spin and Spin-Orbit Effects, Phys. Rev. 147 (1966) 295.
[91] G. Blatter, V. B. Geshkenbein, A. I. Larkin, From isotropic to anisotropic superconductors: A scaling approach, Phys. Rev. Lett. 68 (1992) 875.
[92] L. Jiao, Z. F. Weng, J. Z. Liu, J. L. Zhang, G. M. Pang, C. Y. Guo, F. Gao, X. Y. Zhu, H. H. Wen, H. Q. Yuan, BCS-like superconductivity in $NdO_{1-x}F_xBiS_2$ (x = 0.3 and 0.5) single crystals (2014). arXiv:1406.6791v1.
[93] C. M. Varma, Theory of the pseudogap state of the cuprates, Phys. Rev. B 73 (2006) 155113.
[94] M. M. Qazilbash, J. J. Hamlin, R. E. Baumbach, L. Zhang, D. J. Singh, M. B. Maple, D. N. Basov, Electronic correlations in the iron pnictides, Nat. Phys. 5 (2009) 647.
[95] C. A. McElroy, manuscript in preperation.
[96] R. Kumar, manuscript in preperation.
[97] R. Jha, H. Tiwari, V. P. S. Awana, Appearance of bulk superconductivity under hydrostatic pressure in $Sr_{0.5}RE_{0.5}FBiS_2$ (RE = Ce, Nd, Pr, and Sm) new compounds (2014). arXiv:1407.3105.
[98] J. Kajitani, A. Omachi, T. Hiroi, O. Miura, Y. Mizuguchi, Chemical pressure effect on T_c in BiS_2-based $Ce_{1-x}Nd_xO_{0.5}F_{0.5}BiS_2$, Physica C 504 (2014) 33.
[99] J. Kajitani, T. Hiroi, A. Omachi, O. Miura, Y. Mizuguchi, Chemical pressure effect on superconductivity of BiS_2-based $Ce_{1-x}Nd_xO_{1-y}F_yBiS_2$ and $Nd_{1-z}Sm_zO_{1-y}F_yBiS_2$ (2014). arXiv:1408.2625.
[100] T. Hiroi, J. Kajitani, A. Omachi, O. Miura, Y. Mizuguchi, Element Substitution Effect on Superconductivity in BiS_2-Based $NdO_{1-x}F_xBiS_2$ (2014). arXiv:1404.6359.